This article has been accepted for publication in a future issue of this journal, but has not been fully edited. Content may change prior to final publication. Citation information: DOI 10.1109/TSG.2019.2911996, IEEE Transactions on Smart Grid

A Framework for Multi-regional Real-time Pricing in Distribution Grids

Kai Zhang, *Student Member, IEEE,* Sarmad Hanif, *Member, IEEE,* Christoph M. Hackl, *Senior Member, IEEE,* Thomas Hamacher

***Abstract*—A novel real-time distributed market framework at the distribution grid level is proposed in this work. The framework coordinates information in a hierarchical manner, while aiming to achieve consensus by sharing physically coupled information among multiple regional operators. In principle, each region maximizes its individual social-welfare problem, which is the local (regional) version of the overall social-welfare maximization of the distribution grid. The individual problem incorporates the coupled physical information from its neighboring regions. The consensus among all regions is then enforced through the proposed Consensus-Alternating direction method of multipliers Structured Trust-region (CAST) algorithm. Upon achieving convergence, the distribution locational marginal price (DLMP) is recovered for each region, which is novel in a sense that on one hand it is computed in a distributed manner, i.e. with preserving local information, and on another hand it accurately represents loss allocation from its neighboring regions. The proposed methodologies are tested on an IEEE 33-bus distribution grid and on a 144-bus network with 5 regions.**

***Index Terms*—Real-time market, alternating direction method of multipliers (ADMM), distributed generator (DG), DLMP, multi-regional operation**

I. Introduction

In view of renewable integration and market liberalization at the distribution grid level, there is an increasing interest in proposing decentralized grid operation [1]. However, the proposed small-scale renewable generations are operated in distribution grids, necessitating new control technologies along with market frameworks for their cost-effective integration. In this paper, we focus on one of these market frameworks, as distribution grids cannot be simply integrated in the current transmission level markets [2]. Fundamentally, this difference originates from the fact that distribution grids have i) higher nonlinearities in their power flow, and ii) larger node numbers compared to transmission grids.

Compared to the centralized system, decentralized grid operation has been shown to be advantageous in terms of computation efficiency, modularity, scalability, and privacy [1]. Moreover, emerging technologies like microgrids (MGs) and virtual power plants (VPPs) provide opportunities for decentralized/distributed frameworks for operating the clustering of geographically-closed distributed generators (DGs), energy storage units and small residential loads. An important part of these frameworks is also a proposal to promote decentralized/distributed energy trading [3]. Due to the geographical restrictions/regulations of energy resources, decentralized energy markets need to be accompanied by regional Distribution System Operator (DSOs), independent entities, with the task of operating their local regions in a safe and secure manner and monitoring their power flows from the neighboring regions. Note that the notion of assigning the DSO to coordinate its available flexibility resources aligns with the efforts of promoting the DSO to adopt a more active role in the future distribution grids [4]. There has not been a great amount of work done on addressing the issues related to such a decentralized system with multi-regional DSOs, which is the proposed framework of this paper.

In line with the above argument, the majority of the literature naturally assigns the DSO to operate the distribution grid market and maximize social welfare (see e.g., [2], [5]–[8]). The state-of-art work in distribution locational marginal price (DLMP) mainly focuses on the computation, composition and interpretation of DLMP [2]. References [8], [9] provide a DLMP model obtained from a linearized optimal power flow (OPF) with features such as congestion management and a multi-period energy-dispatch model for a day-ahead market. However, power flow linearization in [8], [9] inflicts an error in calculating DLMPs, removed in [7] by using a trust-region algorithm. Moreover, it is shown that the trust-region based methodology yields a tractable solution along with DLMP decomposition into loss, congestion and voltage components. Alternative DLMP models are proposed in [3], [10], [11] using convexified load-flow models which suffer from the drawbacks of lack of straight-forward interpretation as discussed in [2], [7]. More specifically, the DLMP decomposition based on the formulation of the relaxation of AC optimal power flow (ACOPF) results in a recursive formula that potentially leads to incorrect interpretations of marginal change in distribution grids [2], [7]. With regard to distributed price calculations, a price-based control framework named as a DLMP framework has been proposed earlier in [12]–[14]. The subgradient algorithm is adopted to achieve a distributed implementation to protect the information privacy of market participants in [12], [13], though with a direct-current power-flow model inflicting a large error in low voltage networks. The work in [14] uses a distributed online pricing scheme using the primal-dual method, where the prices are devised

K. Zhang is with TUM CREATE Limited, Singapore 138602, e-mail: kai.zhang@tum-create.edu.sg

S. Hanif is with Pacific Northwest National Laboratory, while the work is done during his affiliation with TUMCREATE Limited.

C. M. Hackl is with Munich University of Applied Sciences, Germany.

T. Hamacher is with Technical University Munich, Germany.

This work was financially supported by the Singapore National Research Foundation under its Campus for Research Excellence And Technological Enterprise (CREATE) programme.

This article has been accepted for publication in a future issue of this journal, but has not been fully edited. Content may change prior to final publication. Citation information: DOI 10.1109/TSG.2019.2911996, IEEE Transactions on Smart Grid

as the online incentive control signal. To our knowledge, the authors in [14] (i) used a static linear approximation of power flow and (ii) organized the framework in terms of only an operator and end consumers. Both considerations come with drawbacks. Drawback (i) is related to the fact that static linear approximations inflict errors as compared to the actual power flow [7]–[9]. Drawback (ii) arises from the fact that no coordination is provided when the grid is operated by multi-region DSOs, which only have access to local information and physically connected neighbors. Reference [11] proposed a three-level hierarchical market framework consisting of a transmission system operator (TSO), DSOs and local aggregators without the coordination of operators in the distribution grid being handled. An earlier work [3] shed light on this issue and discussed the implementation of distributed DLMP using convexified load flow models. However, all these works [3], [11], [14] do not address the effect on the price due to physically connected neighboring regions, i.e. the effect of coupled losses, which is one of the main goals of this paper.

We propose a distributed DLMP implementation in distribution grids, which provides a framework for multi-regional real-time markets in distribution grids. We adopt a similar regional concept from the transmission grid level [15]–[17] and apply it to the distribution grids. The proposed framework is novel in the sense that it allows the parallelization of clearing the distribution grid market while preserving solution accuracy and privacy. The key contributions of this paper are outlined below:

- The essential ingredient to achieve an accurate DLMP calculation is to solve the ACOPF. Among all the existing techniques dealing with the nonlinearity and nonconvexity (e.g. linearized or convexified power flow), nonlinear programming techniques like the trust region (TR) algorithm turn out to deliver an accurate interpretation of DLMP, along with decomposition in its respective losses, congestion and voltage control [7]. With the progress in distributed optimization solvers, in particular alternating direction method of multipliers (ADMM) [18], [19], we are able to combine the nonlinear programming technique and alternating direction method of multipliers (ADMM) in solving the ACOPF problems. The proposed framework comes with a parallel regulation and computation architecture to overcome the computational burdens caused by the large node number in distribution grids.
- Furthermore, the proposed consensus-ADMM structured TR (CAST) algorithm possesses many other favored features, like a tractable solution and formulation to enable online implementation. That is to say that at each TR iteration, a feasible power flow solution as well as price signals can be recovered in each independent region. In light of this, the proposed CAST algorithm can be used to drill down to seconds scale (see Table IV) and to generate real-time incentive signals and interact with the controllable devices continuously.
- The DLMP calculation has been fully distributed into each region while only limited information exchange is required. We derive the multi-regional injection sensitivity to describe the influence between regions to achieve the distributed DLMP computation. The derived sensitivity only reveals physical information on the coupled buses between regions, therefore, the regional operation autonomy is preserved. The hierarchical information flow is further defined with respect to the communication network requirements.

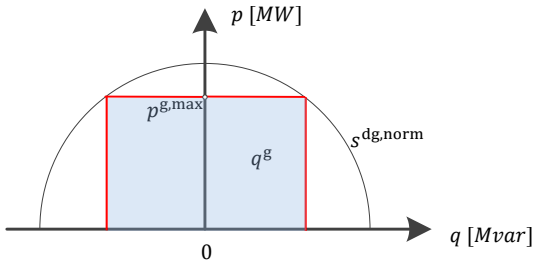

Fig. 1. The range of dispatchable q^{g} in dependence of p^{g} and the nominal power $s^{\mathrm{dg,nom}}$ for photovoltaic generators [21]. The nominal apparent power $s^{\mathrm{dg,nom}}$ is preset to a value which is larger than the maximally admissible value of the active power $p^{\mathrm{g,max}}$ to obtain a time-invariant set for the reactive power (as approximation), i.e. $q^{\mathrm{g}} \leq \sqrt{(s^{\mathrm{dg,nom}})^2 - (p^{\mathrm{g,max}})^2} := \kappa s^{\mathrm{dg,nom}}$.

Notations: $\mathbb{R}$ and $\mathbb{C}$ denote the set of real and complex numbers. Scalars are small letters, i.e. x. Vectors and matrices are in bold letters, i.e. $\mathbf{x}, \mathbf{X}$. Entries of a matrix $\mathbf{X}$ are specified by $X_{i,j}$. Entries of vector $\mathbf{x}$ are specified by x_i whereas the regional version of $\mathbf{x}$ is given as $\mathbf{x}_i$. Conjugates of a complex scalar, vector or matrix are denoted by $\underline{x}, \underline{\mathbf{x}}, \underline{\mathbf{X}}$. The obtained optimal solutions are denoted as $x^*, \mathbf{x}^*$. For complex scalars, vectors or matrices, $\Re(), \Im()$ are used to extract the real and imaginary part. The transpose of a vector or matrix is denoted by $()^\intercal$ and $\mathrm{diag}(\mathbf{x})$ constructs a diagonal matrix with entries of $\mathbf{x}$.

II. Problem Setup

A. Grid Model

We consider a balanced distribution grid. The root bus with index 0 is modeled as a slack node that refers to the power supply point (PSP) connected to the transmission grid. The rest of the nodes are modeled as PQ buses contained in the set $\mathcal{L} := \{1, 2, ..., n\}$ and for all grid nodes we obtain the set $\mathcal{N} := \mathcal{L} \cup \{0\}$. For all grid nodes, we have complex injections and voltage as $\mathbf{s} := \mathbf{p} + \mathrm{j}\mathbf{q}$ and $\mathbf{u} := \mathbf{v} \cdot \mathbf{e}^{\mathrm{j}\boldsymbol{\theta}}$ all with size $\mathbb{C}^{n+1}$, where vectors associated to PQ buses are given as $\mathbf{s}_{\mathcal{L}}, \mathbf{u}_{\mathcal{L}} \in \mathbb{C}^n$ and the individual node $i \in \mathcal{N}$ defines $s_i := p_i + \mathrm{j}q_i$ and $u_i = v_i e^{\mathrm{j}\theta_i}$. Note that active and reactive power for the entire grid consists of $\mathbf{p} = (p_0, \mathbf{p}_{\mathcal{L}}^\intercal)^\intercal$, $\mathbf{q} = (q_0, \mathbf{q}_{\mathcal{L}}^\intercal)^\intercal$. The grid is modeled using the admittance matrix $\mathbf{Y} \in \mathbb{C}^{(n+1)\times(n+1)}$, giving us the following nodal injections to be satisfied [20]:

$$\mathbf{s} = \mathbf{p} + \mathrm{j}\mathbf{q} = \mathrm{diag}(\mathbf{u})\underline{\mathbf{Y}}\,\underline{\mathbf{u}}. \tag{1}$$

In the context of a deregulated real-time distribution level market, we consider DGs (e.g. PV or wind turbine systems) with a full-scale grid-side inverter which, within the DG's power rating, which allows the reactive power to be controlled independently from the active power [22, ch. 3]. Furthermore, energy storage systems (ESS) are assumed to be part of the DG system to buffer the renewable energy output and help the DG

This article has been accepted for publication in a future issue of this journal, but has not been fully edited. Content may change prior to final publication. Citation information: DOI 10.1109/TSG.2019.2911996, IEEE Transactions on Smart Grid

operators to follow the power generation trajectory [23][1]. The DG reactive power output is limited by a ratio κ to its nominal apparent power denoted as $\mathbf{s}^{\text{dg,nom}}$ of the DG system (i.e., the reactive output is constrained by $[-\kappa\mathbf{s}^{\text{dg,nom}}, \kappa\mathbf{s}^{\text{dg,nom}}]$). We illustrate the dispatchable reactive power for a typical DG in Fig. 1. The reactive power capability of a DG unit (e.g. photo-voltaic generators) is in general limited by its nominal apparent power capability $\mathbf{s}^{\text{dg,nom}}$ and the instantaneous time-varying active power p^{g} (i.e. $q^{\text{g}} \leq \sqrt{(s^{\text{dg,nom}})^2 - (p^{\text{g}})^2}$), which makes the reactive power injection time-varying and complicates the optimization problem. To tackle this, the nominal apparent power capability $\mathbf{s}^{\text{dg,nom}}$ of the inverter is advocated to be larger than the maximal active power $p^{\text{g,max}}$, such that enough freedom can be provided for reactive power dispatch in most cases [21], [24]. A reasonable value for oversizing the inverter is e.g. $\mathbf{s}^{\text{dg,nom}} = 1.1p^{\text{g,max}}$ such that $q^{\text{g}} \leq 0.45p^{\text{g,max}}$ [21]. With a *time-invariant approximation*, the feasible region of the dispatchable reactive power q^{g} is obtained as a constrained area regardless of the active power injections of the DG unit. Let $\mathbf{p}^{\text{sl}}, \mathbf{q}^{\text{sl}} \in \mathbb{R}^n$ denote the static load in the grid, then active and reactive nodal injection at PQ buses considering the load and generation are: $\mathbf{p}_{\mathcal{L}} = \mathbf{p}^{\text{g}} - \mathbf{p}^{\text{sl}}$ and $\mathbf{q}_{\mathcal{L}} = \mathbf{q}^{\text{g}} - \mathbf{q}^{\text{sl}}$. Hence, for $\mathbf{p}^{\text{g}} \in \mathbb{R}^n, \mathbf{q}^{\text{g}} \in \mathbb{R}^n$, being the active and reactive power output vectors of all grid-side inverters of DGs[2], we obtain their box constraints as: $[\underline{\mathbf{p}}, \overline{\mathbf{p}}], [\underline{\mathbf{q}}, \overline{\mathbf{q}}]$. The total system active p^{loss} and reactive power q^{loss} losses can be written as [7]:

$$p^{\text{loss}} + \mathrm{j}q^{\text{loss}} = \mathbf{u}^\intercal \underline{\mathbf{Y}}\, \underline{\mathbf{u}} \tag{2}$$

B. Central Optimization Problem

All market participants are assumed to be economically rational and hence seek the maximization of their individual economic surplus. The power delivered to the distribution grid is either through its PSPs or distributed energy resources (DERs), giving the total cost of energy procurement as:

$$w(\mathbf{p}^{\text{g}}, \mathbf{q}^{\text{g}}) = \mathbf{b}^\intercal(p_0, (\mathbf{p}^{\text{g}})^\intercal)^\intercal + \mathbf{d}^\intercal(q_0, (\mathbf{q}^{\text{g}})^\intercal)^\intercal \tag{3}$$

where $\mathbf{b} = (b_0, \mathbf{b}_{\mathcal{L}}^\intercal)^\intercal$ and $\mathbf{d} = (d_0, \mathbf{d}_{\mathcal{L}}^\intercal)^\intercal$ are the locational price vectors (both in $\mathbb{R}^{n+1}$) for active/reactive power procurement, respectively. In particular, c_0 and d_0 are the locational marginal prices at PSP obtained from the wholesale market. To this end, the overall constrained social-welfare maximization problem for the whole grid is given by

$$\text{max.} \quad f(\mathbf{p}^{\text{g}}, \mathbf{q}^{\text{g}}) := -\Big(\mathbf{b}_{\mathcal{L}}^\intercal \mathbf{p}^{\text{sl}} + \mathbf{d}_{\mathcal{L}}^\intercal \mathbf{q}^{\text{sl}} + w(\mathbf{p}^{\text{g}}, \mathbf{q}^{\text{g}})\Big) \tag{4a}$$

$$\text{s.t.} \quad p_0 + \mathbf{1}_n^\intercal \mathbf{p}^{\text{g}} - \mathbf{1}_n^\intercal \mathbf{p}^{\text{sl}} = p^{\text{loss}} \quad : \mu^{\text{pl}} \tag{4b}$$

$$q_0 + \mathbf{1}_n^\intercal \mathbf{q}^{\text{g}} - \mathbf{1}_n^\intercal \mathbf{q}^{\text{sl}} = q^{\text{loss}} \quad : \mu^{\text{ql}} \tag{4c}$$

$$\underline{\mathbf{p}} \leq \mathbf{p}^{\text{g}} \leq \overline{\mathbf{p}} \quad : \underline{\boldsymbol{\mu}}^{\text{p}}, \overline{\boldsymbol{\mu}}^{\text{p}} \tag{4d}$$

$$\underline{\mathbf{q}} \leq \mathbf{q}^{\text{g}} \leq \overline{\mathbf{q}} \quad : \underline{\boldsymbol{\mu}}^{\text{q}}, \overline{\boldsymbol{\mu}}^{\text{q}} \tag{4e}$$

$$\underline{\mathbf{v}} \leq \mathbf{v} \leq \overline{\mathbf{v}} \quad : \underline{\boldsymbol{\mu}}^{\text{v}}, \overline{\boldsymbol{\mu}}^{\text{v}} \tag{4f}$$

[1]This is not a common assumption in literature. Indeed, many proposals are based on the energy storage system to deal with the stochastic nature of renewable generations.

[2]For notational brevity, the dimension of the vectors $\mathbf{p}^{\text{g}}$ and $\mathbf{q}^{\text{g}}$ equals the number of PQ buses.

where, under the assumption of no extra utility exists in satisfying the static load, the maximum social welfare in (4a) is written as the minimum cost of purchasing energy or producing energy [7]. Note that in the literature, social welfare is commonly formulated as the utility benefits minus the generation costs of the supplier [25]. To this end, the benefits for the non-dispatchable static load is obtained as the negative benefits. Constraint (4b)/(4c) is the active/reactive power balance equations. Constraints (4d) to (4f) are box constraints for power dispatches and voltage magnitude limitation. Note that constraints (4b) and (4c) contain the power flow equation implicitly.

In order to obtain the DLMP from the overall problem 4, consider the following Lagrangian function:

$$\begin{aligned} L =& f(\mathbf{p}^{\text{g}}, \mathbf{q}^{\text{g}}) + \mu^{\text{pl}}(p_0 + \mathbf{1}_n^\intercal \mathbf{p}^{\text{g}} - \mathbf{1}_n^\intercal \mathbf{p}^{\text{sl}} - p^{\text{loss}}) + \overline{\boldsymbol{\mu}}^{\text{p}}(\mathbf{p}^{\text{g}} - \overline{\mathbf{p}}) \\ &+ \mu^{\text{ql}}(q_0 + \mathbf{1}_n^\intercal \mathbf{q}^{\text{g}} - \mathbf{1}_n^\intercal \mathbf{q}^{\text{sl}} - q^{\text{loss}}) + \underline{\boldsymbol{\mu}}^{\text{p}}(\mathbf{p}^{\text{g}} - \underline{\mathbf{p}}) \\ &+ (\underline{\boldsymbol{\mu}}^{\text{q}})^\intercal(\mathbf{q}^{\text{g}} - \underline{\mathbf{q}}) + (\overline{\boldsymbol{\mu}}^{\text{q}})^\intercal(\mathbf{q}^{\text{g}} - \overline{\mathbf{q}}) + (\underline{\boldsymbol{\mu}}^{\text{v}})^\intercal(\mathbf{v} - \underline{\mathbf{v}}) \\ &+ (\overline{\boldsymbol{\mu}}^{\text{v}})^\intercal(\mathbf{v} - \overline{\mathbf{v}}). \end{aligned} \tag{5}$$

For the solution of (4), we obtain DLMPs using the first-order derivative of the Lagrangian function for nodal active/reactive power $\boldsymbol{\Pi}^{\text{p}}, \boldsymbol{\Pi}^{\text{q}} \in \mathbb{R}^n$ as the sum of three components [7]:

$$\boldsymbol{\Pi}^{\text{p}} = \boldsymbol{\Pi}^{\text{p,e}} + \boldsymbol{\Pi}^{\text{p,l}} + \boldsymbol{\Pi}^{\text{p,v}}, \tag{6}$$

where (i) $\boldsymbol{\Pi}^{\text{p,e}} := b_0\mathbf{1}_n$ is the energy component, (ii) $\boldsymbol{\Pi}^{\text{p,l}} := -((\mathbf{m}_{\mathcal{L}}^{\text{pl,p}})^\intercal b_0 + (\mathbf{m}_{\mathcal{L}}^{\text{ql,p}})^\intercal d_0)$ is the loss component with $\mathbf{m}_{\mathcal{L}}^{\text{pl,p}}, \mathbf{m}_{\mathcal{L}}^{\text{ql,p}} \in \mathbb{R}^{1\times n}$ as the loss sensitivity coefficient (see Appendix A for derivation) and, (iii) $\boldsymbol{\Pi}^{\text{p,v}} := (\mathbf{M}_{\mathcal{L}}^{\text{vp}})^\intercal(\underline{\boldsymbol{\mu}}^{\text{v}} - \overline{\boldsymbol{\mu}}^{\text{v}})$ is the voltage support component with $\mathbf{M}_{\mathcal{L}}^{\text{vp}} \in \mathbb{R}^{n\times n}$ as the voltage sensitivity with respect to active power. DLMPs for reactive power can be derived in a similar way.

Remark II.1 (DLMP with renewables)**.** *Suppose that a mechanism exists to monetize services from renewables. For example using aggregated voltage support from a group of inverters' reactive powers [22, ch. 3]. Then, similar to generic DGs, this mechanism can be simply treated as marginal cost bids and included in the objective function* (4a)*. However, as renewables are usually associated with zero (short-term) marginal cost, so that they can be utilized to their full availability, we simply represent them as constant PQ generation injection, as mentioned in Section II-A.*

Remark II.2 (DLMP under uncertainties)**.** *The proposed DLMP framework of* (4) *is deterministic, i.e., it does not contain any uncertainties in its injections (loads/generations). For calculating DLMPs, our previous work [12] discusses methods to cast these uncertainties in a deterministic form. As dealing with uncertainties is not the focus of this paper, it is not considered here. However, formulation compatibility of the proposed framework to include such formulations is discussed in detail in Section IV-B4.*

C. Problem Statement

In order to consider the proposed market framework of Fig. 2, we now envision the distribution grid to be operated by multiple regional DSOs. The goal of this framework is

This article has been accepted for publication in a future issue of this journal, but has not been fully edited. Content may change prior to final publication. Citation information: DOI 10.1109/TSG.2019.2911996, IEEE Transactions on Smart Grid

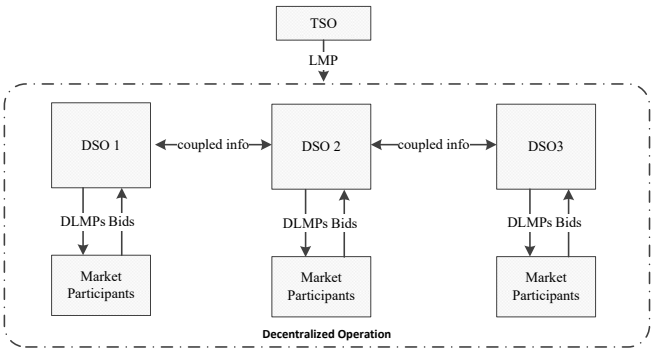

Fig. 2. Proposed market framework and information flow diagram.

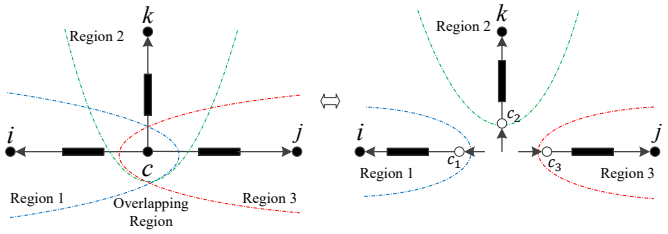

Fig. 3. Network-partitioning technique and consensus definition for multiple regions (dashed lines are the regions' boundary).

then to coordinate the DSOs such that they maximize the overall social welfare of the distribution grid while maximizing their individual surplus. Moreover, each regional DSO must be independent in making its decision and only share physically connected bus power flow information with the neighboring region's DSO. Similar to the overall problem 4, DERs (such as DGs, ESSs) are assumed to be price takers and receive rewards from the associated regional DSO for power generations. However, in order to achieve the proposed distributed framework of Fig. 2 along with the price structure of (6), two research questions exist, which are answered in this proposed work. Firstly, we solve the ACOPF problem imposed by (4) in a distributed way, preserving private information of the regional DSO. Secondly, we obtain DLMP for each region in a distributed manner with the similar decomposition structure of (6) and optimality of (4), as when solved centrally.

III. Market Framework - CAST Algorithm

A. Network Partitioning Technique and Consensus Definition

The distribution network is partitioned into r regions where the set of regions is denoted by $\mathcal{R} = \{1, 2, ..., r\}$. Similarly, the overall PQ bus set $\mathcal{L}$ gets partitioned into r subsets, $\mathcal{L}_i := \{1_i, 2_i, ..., n_i\}$, where $i \in \mathcal{R}$. To enforce feasibility with respect to the overall grid, each region i places a reference bus (slack bus) at its physically connected neighbor. Hence, we get $\mathcal{N}_i = \mathcal{L}_i \cup \{0\}$ total nodes in the region. With this, each region i can now be represented with its local $\mathbf{Y}_i \in \mathbb{C}^{(n_i+1)\times(n_i+1)}$ and individual objective function $f_i(\mathbf{p}^{\mathrm{g}}_{\mathcal{L}_i}, \mathbf{q}^{\mathrm{g}}_{\mathcal{L}_i})$, which are the respective local versions of the overall objective function $f(\mathbf{p}^{\mathrm{g}}, \mathbf{q}^{\mathrm{g}})$ and system admittance matrix $\mathbf{Y}$.

The interconnection between regions is established by overlapping areas in which the power flow equations of each region can be interlinked. If region i is a neighbor of region j, then $\mathcal{N}_i \cap \mathcal{N}_j \neq \emptyset, \forall i, j \in \mathcal{R}$, such that $\mathcal{N}_i \cap \mathcal{N}_j$ gives a set of coupled buses that interconnects region i and region j. The set $\mathcal{C}_{ij} := \{c_{i_1} = c_{j_1}, \ldots, c_{i_k} = c_{j_k}\}$ denotes the set of k coupled buses from regions i and j (where $k < \max\{n_i, n_j\}$). In Fig. 3 (left), an example of a coupled bus of three regions is illustrated. The bus $c := c_1 = c_2 = c_3$ is part of region 1 (c_1), region 2 (c_2) and region 3 (c_3). Hence, $\mathcal{C}_{12} = \{c_1 = c_2\}$, $\mathcal{C}_{13} = \{c_1 = c_3\}$ and $\mathcal{C}_{23} = \{c_2 = c_3\}$.

In order to decouple the constraints for the optimization problem in (4) and to solve it in a distributed way, the objective and constraints are decoupled with the help of local copies of the coupled buses created for each region. To do so, we define the set of the local copies of the coupled buses in region i as $\mathcal{C}_i := \cap_{j=1}^{r} \mathcal{C}_{ij} \subset \mathcal{N}_i$. For any local copy $c_i \in \mathcal{C}_i$, the number of connected neighboring regions is specified by n_{c_i}. For example, in Fig. 3, three local copies of the coupled bus c are created and denoted by c_1, c_2, c_3 which gives $\mathcal{C}_1 = \{c_1, c_2, c_3\}$ and $n_{c_1} = 3$.

To enforce the agreement on the power flow on the coupled buses among regions, the following consensus constraints are introduced for region $i \in \mathcal{R}$ as

$$v_{c_1} = v_{c_2} = ... = v_{c_{n_{c_i}}} \qquad c_i \in \mathcal{C}_i \qquad (7a)$$

$$\theta_{c_1} = \theta_{c_2} = ... = \theta_{c_{n_{c_i}}} \qquad c_i \in \mathcal{C}_i \qquad (7b)$$

$$\sum_{i=1}^{n_{c_i}} p_{c_i} = 0 \qquad c_i \in \mathcal{C}_i \qquad (7c)$$

$$\sum_{i=1}^{n_{c_i}} q_{c_i} = 0 \qquad c_i \in \mathcal{C}_i. \qquad (7d)$$

B. Consensus Optimal Power Flow (Consensus OPF)

Along with the network partition, problem (4) is decomposed into regional subproblems. For a region $i \in \mathcal{R}$, the following consensus optimization problem is defined

$$\max. \quad f_i(\mathbf{p}^{\mathrm{g}}_{\mathcal{L}_i}, \mathbf{q}^{\mathrm{g}}_{\mathcal{L}_i}) \qquad (8a)$$

$$\text{s.t.} \quad p_{0,i} + \mathbf{1}^{\intercal}_{n_i} \mathbf{p}^{\mathrm{g}}_{\mathcal{L}_i} - \mathbf{1}^{\intercal}_{n_i} \mathbf{p}^{\mathrm{sl}}_{\mathcal{L}_i} = p^{\mathrm{loss}}_i \qquad : \mu^{\mathrm{pl}}_i \qquad (8b)$$

$$q_{0,i} + \mathbf{1}^{\intercal}_{n_i} \mathbf{q}^{\mathrm{g}}_{\mathcal{L}_i} - \mathbf{1}^{\intercal}_{n_i} \mathbf{q}^{\mathrm{sl}}_{\mathcal{L}_i} = q^{\mathrm{loss}}_i \qquad : \mu^{\mathrm{ql}}_i \qquad (8c)$$

$$\underline{\mathbf{p}}_{\mathcal{L}_i} \leq \mathbf{p}^{\mathrm{g}}_{\mathcal{L}_i} \leq \overline{\mathbf{p}}_{\mathcal{L}_i} \qquad : \underline{\boldsymbol{\mu}}^{\mathrm{p}}_i, \overline{\boldsymbol{\mu}}^{\mathrm{p}}_i \qquad (8d)$$

$$\underline{\mathbf{q}}_{\mathcal{L}_i} \leq \mathbf{q}^{\mathrm{g}}_{\mathcal{L}_i} \leq \overline{\mathbf{q}}_{\mathcal{L}_i} \qquad : \underline{\boldsymbol{\mu}}^{\mathrm{q}}_i, \overline{\boldsymbol{\mu}}^{\mathrm{q}}_i \qquad (8e)$$

$$\underline{\mathbf{v}}_{\mathcal{L}_i} \leq \mathbf{v}_{\mathcal{L}_i} \leq \overline{\mathbf{v}}_{\mathcal{L}_i} \qquad : \underline{\boldsymbol{\mu}}^{\mathrm{v}}_i, \overline{\boldsymbol{\mu}}^{\mathrm{v}}_i \qquad (8f)$$

and (7a) to (7d),

where the constraints (8b) and (8c) are regional representation of constraints (4b) and (4c). Consensus constraints (7a) to (7d) ensure that the power flow still holds for the global optimization problem and require each region to take into account binding its power injection at coupled buses with respect to its global values provided from other regions. In the next section, we elaborate how to solve the consensus OPF and tackle the power flow nonlinearity in the proposed CAST algorithm.

This article has been accepted for publication in a future issue of this journal, but has not been fully edited. Content may change prior to final publication. Citation information: DOI 10.1109/TSG.2019.2911996, IEEE Transactions on Smart Grid

C. Distributed Solver with CAST Algorithm

The proposed CAST algorithm possesses a ADMM structure with TR algorithm embedded at each ADMM iteration as the local optimization solver. Note that each local optimization solver handles a regional subproblem with nonlinear AC power flow constraint (1) which is tackled by TR algorithm. The fundamental idea of the trust region algorithm is to create an approximate model (linear model) for the initial operating point within a feasible region (trust region). Then the minimization step helps to find the steepest descent direction along the objective function within the trust region. In a new iteration, the linearized model is then updated using the new operating point found in the steepest descent direction. The algorithm repeats the steps until no further improvement can be found within the next minimization step. Note that the trust region is adjusted from iteration to iteration, i.e., the trust region will be enlarged if the approximate model represents the original problem well and vice versa.

ADMM is a distributed solver mainly for convex optimization problems [26]. In principle, ADMM relies on the augmented Lagrangian to reduce the mismatch of the coupled constraints (7a) to (7d) iteratively when each local optimization solver solves the subproblem. ADMM has been proven to work well for solving ACOPF as well as other nonlinear problems despite nonconvexity [19]. Interested readers may refer to [27] for alternative distributed ACOPF algorithms. In this work, the proposed CAST algorithm can be considered as a variant of the distributed ACOPF solver in [18], [19] with the main distinction of being the use of a trust-region method instead of an interior point method (IPM) as the local minimization solver. This, however, does not change the convergence guarantee nor the optimality conditions. The convergence speed of the CAST algorithm is furthermore improved by using the varying penalty (VP) method [26], [28] i.e., during the ADMM parameter update stage, by utilizing the primal/dual residual information that measures the local and global minimization progress respectively, the penalty factor will be changed accordingly at each iteration, and hence convergence performance is improved. We provide the validation of the VP method in the numerical experiment.

Consider the augmented Lagrangian of a region $i \in \mathcal{R}$ as:

$$\begin{aligned} L_i^{\text{ADMM}}(\tilde{\boldsymbol{\chi}}_{\mathcal{L}_i}) =& f_i(\tilde{\mathbf{p}}^{\text{g}}_{\mathcal{L}_i}, \tilde{\mathbf{q}}^{\text{g}}_{\mathcal{L}_i}) + \boldsymbol{\lambda}_i^{\intercal}(\tilde{\boldsymbol{\chi}}_{\mathcal{C}_i} - \tilde{\boldsymbol{\chi}}^{+}_{\mathcal{C}_i}) \\ &+ \frac{1}{2}\rho_i(\tilde{\boldsymbol{\chi}}_{\mathcal{C}_i} - \tilde{\boldsymbol{\chi}}^{+}_{\mathcal{C}_i})^{\intercal}(\tilde{\boldsymbol{\chi}}_{\mathcal{C}_i} - \tilde{\boldsymbol{\chi}}^{+}_{\mathcal{C}_i}) \end{aligned} \tag{9}$$

with decision variables for node i defined by $\boldsymbol{\chi}_i := [p_i, q_i, v_i] \in \mathbb{R}^3$, Lagrange multiplier $\boldsymbol{\lambda}_i \in \mathbb{R}^{3n_{c_i}}$ and the penalty factor $\rho_i \in \mathbb{R}$. We consider injection and voltage magnitudes as the coupling variables here, because angles for each region are implicitly updated locally with respect to the given coupled bus c_i, serving as its slack bus (see Sec. III-A on assumptions in network partitioning). Moreover, $\tilde{\boldsymbol{\chi}}^{+}_{\mathcal{C}_i} \in \mathbb{R}^{2n_{c_i}}$ denotes the global variable to be updated based on the local optimization results at each ADMM iteration. The nonlinearities in (8) are approximated by using (local) linear estimates

$$\tilde{\mathbf{v}}_{\mathcal{L}_i} = \hat{\mathbf{v}}_{\mathcal{L}_i} + \mathbf{M}^{\text{vp}}_{\mathcal{L}_i}\Delta\mathbf{p}_{\mathcal{L}_i} + \mathbf{M}^{\text{vq}}_{\mathcal{L}_i}\Delta\mathbf{q}_{\mathcal{L}_i} + \mathbf{m}^{\text{vv}}_{\mathcal{L}_i}\Delta v_{0,i} \tag{10a}$$

$$\tilde{\boldsymbol{\theta}}_{\mathcal{L}_i} = \hat{\boldsymbol{\theta}}_{\mathcal{L}_i} + \mathbf{M}^{\theta p}_{\mathcal{L}_i}\Delta\mathbf{p}_{\mathcal{L}_i} + \mathbf{M}^{\theta q}_{\mathcal{L}_i}\Delta\mathbf{q}_{\mathcal{L}_i} + \mathbf{m}^{\theta v}_{\mathcal{L}_i}\Delta v_{0,i} \tag{10b}$$

$$\tilde{p}_{0,i} = \hat{p}_{0,i} + \mathbf{m}^{\text{pp}}_{\mathcal{L}_i}\Delta\mathbf{p}_{\mathcal{L}_i} + \mathbf{m}^{\text{pq}}_{\mathcal{L}_i}\Delta\mathbf{q}_{\mathcal{L}_i} + m^{\text{pv}}\Delta v_{0,i} \tag{10c}$$

$$\tilde{q}_{0,i} = \hat{q}_{0,i} + \mathbf{m}^{\text{qp}}_{\mathcal{L}_i}\Delta\mathbf{p}_{\mathcal{L}_i} + \mathbf{m}^{\text{qq}}_{\mathcal{L}_i}\Delta\mathbf{q}_{\mathcal{L}_i} + m^{\text{qv}}\Delta v_{0,i} \tag{10d}$$

$$\tilde{v}_{0,i} = \hat{v}_{0,i} + \Delta v_{0,i}, \tag{10e}$$

where a *new* operating point $(\tilde{\mathbf{v}}_{\mathcal{L}_i}, \tilde{\boldsymbol{\theta}}_{\mathcal{L}_i}, \tilde{p}_{0,i}, \tilde{q}_{0,i}, \tilde{v}_{0,i})$ is approximated by the given (old) operating point $(\hat{\mathbf{v}}_{\mathcal{L}_i}, \hat{\boldsymbol{\theta}}_{\mathcal{L}_i}, \hat{p}_{0,i}, \hat{q}_{0,i}, \hat{v}_{0,i})$ using the linearization coefficient matrices or vectors denoted by $\mathbf{M}^{\text{vp}}_{\mathcal{L}_i}, \mathbf{M}^{\text{vq}}_{\mathcal{L}_i}, \mathbf{M}^{\theta p}_{\mathcal{L}_i}, \mathbf{M}^{\theta q}_{\mathcal{L}_i} \in \mathbb{R}^{n_i \times n_i}$, $\mathbf{m}^{\text{pp}}_{\mathcal{L}_i}, \mathbf{m}^{\text{pq}}_{\mathcal{L}_i}, \mathbf{m}^{\text{qp}}_{\mathcal{L}_i}, \mathbf{m}^{\text{qq}}_{\mathcal{L}_i} \in \mathbb{R}^{1 \times n_i}$, $\mathbf{m}^{\text{vv}}_{\mathcal{L}_i}, \mathbf{m}^{\theta v}_{\mathcal{L}_i} \in \mathbb{R}^{n_i \times 1}$, $m^{\text{pv}}, m^{\text{qv}} \in \mathbb{R}$. The derivation of the coefficients are provided in Appendix A. As the linearization of distribution-grid power flows is only accurate at the chosen operating point, we incorporate a trust-region algorithm to tackle the related nonlinearities [7]. Algorithm 1 explains the proposed CAST algorithm, where all computations are performed locally, except for step 2, which requires an update on the algorithm's global variables. The global variables update is followed by the averaging step of using local optimization results of the coupled variable. Interested readers may refer to [26, ch. 7] for the derivation of averaging steps in the ADMM algorithm. This update makes intuitive sense, i.e., upon convergence of CAST, the consensus power flow constraints (7a) to (7d) will be binding. Note that the parameter tuning steps for TR (step 1.4 - 1.5) and for ADMM (step 3.1 - 3.2) are carried out locally by its regional DSO. However, there are other variants of ADMM which require a central entity to update the information and coordinate the parameter tuning (see e.g., [27], [28]).

Remark III.1 (Convergence of CAST algorithm)**.** *Under the condition that the sequence of the penalties ρ_i for all $i \in \mathcal{R}$ is bounded, the convergence of the CAST algorithm can be proved using [18, Theorem 4]. In addition, upon the convergence of the CAST algorithm, the triplets $(\boldsymbol{\lambda}_i, \rho_i, \boldsymbol{\chi}_{\mathcal{L}_i})$ converge to Karush-Kuhn-Tucker (KKT) stationary points [18, Theorem 1] (i.e., local minimum for non-convex scenarios and global minimum for convex scenarios). In practice, the first two steps of CAST algorithm can take place in either order without affecting the convergence. This kind of asynchronous update has proved advantageous in dealing with communication delays and packet loss in recent expositions [30], [31].*

Remark III.2 (Tractable solution and formulation to enable the online implementation)**.** *The trust region ensures a feasible load flow solution to be found at each ADMM iteration, which provides a tractable OPF solution along with the price signal in each region. This feature is favored by many online applications and can be further exploited in the provision of real-time control (see e.g., [32], [33]).*

IV. Market Framework - Multi-Regional DLMPs

In this section, we extend the central price decomposition structure of (6) for physically coupled multi-regions. In doing so, the proposed network reflects the effect of physically coupled regions in their locally calculated price, while keeping

This article has been accepted for publication in a future issue of this journal, but has not been fully edited. Content may change prior to final publication. Citation information: DOI 10.1109/TSG.2019.2911996, IEEE Transactions on Smart Grid

Algorithm 1 CAST algorithm - parallelized in all regions

Input: $\hat{\boldsymbol{\chi}}_{\mathcal{L}_i}(0)$ - initial feasible state variable, $f_i(\hat{\boldsymbol{\chi}}_{\mathcal{L}_i}(0))$ - initial local objective value

Parameters: ϵ - termination tolerance, $\phi_i(k)$ - trust-region radius; $\phi_{\max}$ - maximal trust-region radius; η,β,$\gamma \in (0,1)$ - trust-region constants; τ,κ - ADMM constants;

ADMM loop:

Step 1. (Local minimization with trust-region algorithm)

1.1 Choice of linearized model: to construct/update the sensitivity matrix for linearized power flow model at operational point $(\hat{u}_{\mathcal{L}_i}(k), \hat{s}_0(k))$, i.e., (10a) to (10d).

1.2 Trust region minimization with L_i^{ADMM} as in (9):

$$\tilde{\boldsymbol{\chi}}^*_{\mathcal{L}_i}(k+1) := \arg\min_{\tilde{\boldsymbol{\chi}}_{\mathcal{L}_i}} L_i^{\text{ADMM}} \tag{11a}$$

$$\text{s.t.} \quad \text{(8d) to (8f) and (10a) to (10d)} \tag{11b}$$

$$||\tilde{\boldsymbol{\chi}}_{\mathcal{L}_i}(k+1) - \hat{\boldsymbol{\chi}}_{\mathcal{L}_i}(k)|| < \phi_i \tag{11c}$$

1.3 Feasible power flow projection: the next operational point $\hat{\boldsymbol{\chi}}_{\mathcal{L}_i}(k+1)$ is obtained by projecting the optimization results $\tilde{\boldsymbol{\chi}}^*_{\mathcal{L}_i}(k+1)$ to the feasible power flow solution, e.g. by using a Newton–Raphson algorithm [29].

1.4 With the previous operational point $\hat{\boldsymbol{\chi}}_{\mathcal{L}_i}(k)$, the approximate point $\tilde{\boldsymbol{\chi}}_{\mathcal{L}_i}(k+1)$ and the current operational point $\hat{\boldsymbol{\chi}}_{\mathcal{L}_i}(k+1)$, the following ratio is computed:

$$\sigma_i(k+1) = \frac{L_i^{\text{ADMM}}(\hat{\boldsymbol{\chi}}_{\mathcal{L}_i}(k+1)) - L_i^{\text{ADMM}}(\hat{\boldsymbol{\chi}}_{\mathcal{L}_i}(k))}{L_i^{\text{ADMM}}(\tilde{\boldsymbol{\chi}}^*_{\mathcal{L}_i}(k+1)) - L_i^{\text{ADMM}}(\hat{\boldsymbol{\chi}}_{\mathcal{L}_i}(k))} \tag{12}$$

which represents the ratio between actual objective reduction and predicted reduction.

1.5 Trust region radii evaluation and update:

$$\phi_i(k+1) = \begin{cases} \gamma\phi_i(k) & \sigma_i(k+1) \le \eta \\ \min\{\phi_{\max}, 2\phi_i(k)\} & \sigma_i(k+1) \ge (1-\eta) \\ \phi_i(k) & \text{otherwise} \end{cases}$$

1.6 Trust region solution evaluation:
If $\sigma_i(k+1) > \beta$, solution of $\hat{\boldsymbol{\chi}}_{\mathcal{L}_i}(k+1)$ is accepted, otherwise rejected and $\hat{\boldsymbol{\chi}}_{\mathcal{L}_i}(k+1) = \hat{\boldsymbol{\chi}}_{\mathcal{L}_i}(k)$ is set.

1.7 Termination criteria check of trust region: $||\tilde{\boldsymbol{\chi}}_{\mathcal{L}_i}(k+1) - \hat{\boldsymbol{\chi}}_{\mathcal{L}_i}(k+1)|| < \epsilon$.

Step 2. (Global variable update)

For the coupled buses $c_i \in \mathcal{C}_i$, we have

$$\tilde{\chi}^+_{c_i}(k+1) = \sum_{i=1}^{n_{c_i}} \tilde{\chi}^*_{c_i}(k+1), \tag{13}$$

where the global variables are updated using the average value of the local optimization results. The step requires information exchange between regions, i.e., passing the local optimization results $\tilde{\chi}^*_{c_i}(k+1)$ to connected regions.

Step 3. (ADMM parameter update)

3.1 Primal and dual residual update:
For each region $i \in \mathcal{R}$, the squared primal residual $r_i \in \mathbb{R}$ and dual residual $s_i \in \mathbb{R}$ are updated as follows

$$r_i^2(k+1) = \|\tilde{\boldsymbol{\chi}}^*_{\mathcal{C}_i}(k+1) - \tilde{\boldsymbol{\chi}}^+_{\mathcal{C}_i}(k+1)\|_2^2 \tag{14}$$

$$s_i^2(k+1) = \|\tilde{\boldsymbol{\chi}}^+_{\mathcal{C}_i}(k+1) - \tilde{\boldsymbol{\chi}}^+_{\mathcal{C}_i}(k)\|_2^2. \tag{15}$$

3.2 Penalty factor update:

$$\rho_i(k+1) = \begin{cases} \rho_i(k)\cdot(1+\tau) & r_i(k+1) > \kappa\, s_i(k+1) \\ \rho_i(k)\cdot(1+\tau)^{-1} & r_i(k+1) < \kappa\, s_i(k+1) \\ \rho_i(k) & \text{otherwise,} \end{cases}$$

where $\rho_i \in \mathbb{R}$ is the penalty factor associated to each region $i \in \mathcal{R}$ which is changed at each iteration depending on the local and global consensus progress measured by primal and dual residuals.

3.3 Lagrangian multiplier update step:

$$\boldsymbol{\lambda}_i(k+1) = \boldsymbol{\lambda}_i(k) + \rho_i\big(\hat{\boldsymbol{\chi}}_{\mathcal{C}_i}(k+1) - \tilde{\boldsymbol{\chi}}^+_{\mathcal{C}_i}(k+1)\big). \tag{16}$$

the desired DLMP decomposition in its respective energy, loss and voltage components.

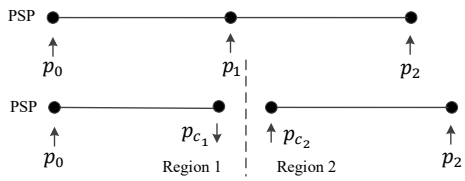

Fig. 4. Three-bus example.

1) Three-bus network example: First, consider centralized active power DLMPs (6) for the exemplary 3-bus system given in Fig. 4, with non-binding voltages

$$b_1 = b_0 - \frac{\partial p^{\text{loss}}}{\partial p_1} b_0 - \frac{\partial q^{\text{loss}}}{\partial p_1} d_0 \quad \text{and} \tag{17}$$

$$b_2 = b_0 - \frac{\partial p^{\text{loss}}}{\partial p_2} b_0 - \frac{\partial q^{\text{loss}}}{\partial p_2} d_0. \tag{18}$$

Note that the following two reasons prevent the adoption of the aforementioned price structure: (i) With the partitioning, note that b_0, originally the marginal price at the slack bus, is now local to region 1. Moreover, region 2 has a new root-bus, i.e., bus c_2. Hence, the formulation needs to be adjusted to account for these structural changes. (ii) Each region only computes local losses through local linearized terms $\mathbf{m}^{\text{pl,p}}_{\mathcal{L}_1}, \mathbf{m}^{\text{ql,p}}_{\mathcal{L}_1}, \mathbf{m}^{\text{pl,p}}_{\mathcal{L}_2}, \mathbf{m}^{\text{ql,p}}_{\mathcal{L}_2}$. However, the losses in the each region are coupled to its neighboring region's injection through the local copies p_{c_1}, p_{c_2}. Hence, if not accounted, this effect might introduce errors in the local loss calculations and its representation in DLMPs. We introduce the distributed DLMP scheme as follows to address these issues. With regard to classification of parent and children region in the distributed DLMP scheme, the following explanation holds. Starting from the region connected to PSP, the regions can be arranged in a sequential order. The region which has a connected downstream region serves as the parent region with its downstream region as the children region. Moreover, the children region might serve as a parent region for its further connected neighbors (children). With this, in Fig. 3, region 1 is the parent and region 2 is the children region.

A. Distributed DLMP Scheme

Distributed DLMP scheme

1.1 For any children region, the root-node price is obtained as the cleared DLMP at the respective parent region's connected node

1.2 For any parent region i, the active power regional DLMPs $\boldsymbol{\Pi}^{\text{p}}_i$ are given as:

$$\boldsymbol{\Pi}^{\text{p}}_i = \boldsymbol{\Pi}^{\text{p,e}}_i + \boldsymbol{\Pi}^{\text{p,l}}_i + \boldsymbol{\Pi}^{\text{p,v}}_i + \boldsymbol{\Pi}^{\text{p,ADMM}}_i \tag{19}$$

with $\boldsymbol{\Pi}^{\text{p,ADMM}}_i = -\big(\frac{\partial \mathbf{p}_{\mathcal{C}_i}}{\partial \mathbf{p}_{\mathcal{L}_i}}, \frac{\partial \mathbf{q}_{\mathcal{C}_i}}{\partial \mathbf{p}_{\mathcal{L}_i}}, \frac{\partial \mathbf{v}_{\mathcal{C}_i}}{\partial \mathbf{p}_{\mathcal{L}_i}}\big)\boldsymbol{\lambda}_i^{\intercal}$ and $\boldsymbol{\Pi}^{\text{p,e}}_i, \boldsymbol{\Pi}^{\text{p,l}}_i, \boldsymbol{\Pi}^{\text{p,v}}_i$ are formulated in the same way as in Section II-B.

The proposed distributed DLMP scheme adapts to the structural changes resulted from network partitioning and the

This article has been accepted for publication in a future issue of this journal, but has not been fully edited. Content may change prior to final publication. Citation information: DOI 10.1109/TSG.2019.2911996, IEEE Transactions on Smart Grid

derivation is provided as follows. The Lagrangian function associated to sub-optimization problem in region i is given as

$$\begin{aligned}
L_i &= f_i + (\boldsymbol{\lambda}_i^{\mathrm{p}})^\intercal(\mathbf{p}_{\mathcal{C}_i} - \mathbf{p}_{\mathcal{C}_i}^+) + (\boldsymbol{\lambda}_i^{\mathrm{q}})^\intercal(\mathbf{q}_{\mathcal{C}_i} - \mathbf{q}_{\mathcal{C}_i}^+) \\
&+ (\boldsymbol{\lambda}_i^{\mathrm{v}})^\intercal(\mathbf{v}_{\mathcal{C}_i} - \mathbf{v}_{\mathcal{C}_i}^+) + \frac{1}{2}\rho_i(\tilde{\mathbf{p}}_{\mathcal{C}_i} - \tilde{\mathbf{p}}_{\mathcal{C}_i}^+)^\intercal(\tilde{\mathbf{p}}_{\mathcal{C}_i} - \tilde{\mathbf{p}}_{\mathcal{C}_i}^+) \\
&+ \frac{1}{2}\rho_i(\tilde{\mathbf{q}}_{\mathcal{C}_i} - \tilde{\mathbf{q}}_{\mathcal{C}_i}^+)^\intercal(\tilde{\mathbf{q}}_{\mathcal{C}_i} - \tilde{\mathbf{q}}_{\mathcal{C}_i}^+) + \frac{1}{2}\rho_i(\tilde{\mathbf{v}}_{\mathcal{C}_i} - \tilde{\mathbf{v}}_{\mathcal{C}_i}^+)^\intercal(\tilde{\mathbf{v}}_{\mathcal{C}_i} - \tilde{\mathbf{v}}_{\mathcal{C}_i}^+) \\
&+ \mu_i^{\mathrm{pl}}(-p_{0,i} - \mathbf{1}_{n_i}^\intercal \mathbf{p}_{\mathcal{L}_i}^{\mathrm{g}} + \mathbf{1}_{n_i}^\intercal \mathbf{p}_{\mathcal{L}_i}^{\mathrm{sl}} + p_i^{\mathrm{loss}}) \\
&+ \mu_i^{\mathrm{ql}}(-q_{0,i} - \mathbf{1}_{n_i}^\intercal \mathbf{q}_{\mathcal{L}_i}^{\mathrm{g}} + \mathbf{1}_{n_i}^\intercal \mathbf{q}_{\mathcal{L}_i}^{\mathrm{sl}} + q_i^{\mathrm{loss}}) \\
&+ (\overline{\boldsymbol{\mu}}_i^{\mathrm{p}})^\intercal(\mathbf{p}_{\mathcal{L}_i}^{\mathrm{g}} - \overline{\mathbf{p}}_{\mathcal{L}_i}) - (\underline{\boldsymbol{\mu}}_i^{\mathrm{p}})^\intercal(\mathbf{p}_{\mathcal{L}_i}^{\mathrm{g}} - \underline{\mathbf{p}}_{\mathcal{L}_i}) \\
&+ (\overline{\boldsymbol{\mu}}_i^{\mathrm{q}})^\intercal(\mathbf{q}_{\mathcal{L}_i}^{\mathrm{g}} - \overline{\mathbf{q}}_{\mathcal{L}_i}) - (\underline{\boldsymbol{\mu}}_i^{\mathrm{q}})^\intercal(\mathbf{q}_{\mathcal{L}_i}^{\mathrm{g}} - \underline{\mathbf{q}}_{\mathcal{L}_i}) \\
&+ (\overline{\boldsymbol{\mu}}_i^{\mathrm{v}})^\intercal(\mathbf{v}_{\mathcal{L}_i} - \overline{\mathbf{v}}_{\mathcal{L}_i}) - (\underline{\boldsymbol{\mu}}_i^{\mathrm{v}})^\intercal(\mathbf{v}_{\mathcal{L}_i} - \underline{\mathbf{v}}_{\mathcal{L}_i}),
\end{aligned} \tag{20}$$

where the Lagrangian multiplier $\boldsymbol{\lambda}_i = [\boldsymbol{\lambda}_i^{\mathrm{p}}, \boldsymbol{\lambda}_i^{\mathrm{q}}, \boldsymbol{\lambda}_i^{\mathrm{v}}]$ consisting of three parts for coupled active power and reactive power. Where $\mathbf{b}_{\mathcal{L}_i}^*, \mathbf{d}_{\mathcal{L}_i}^*$ represent the regional DLMPs for active power and reactive power respectively, the KKT conditions comprise of first-order optimality conditions:

$$\begin{aligned}
&\mathbf{b}_{\mathcal{L}_i}^* + \mu_i^{\mathrm{pl}}(\mathbf{m}_{\mathcal{L}_i}^{\mathrm{pl,p}})^\intercal + \mu_i^{\mathrm{ql}}(\mathbf{m}_{\mathcal{L}_i}^{\mathrm{ql,p}})^\intercal + (\boldsymbol{\lambda}_i^{\mathrm{p}})^\intercal \frac{\partial \mathbf{p}_{\mathcal{C}_i}}{\partial \mathbf{p}_{\mathcal{L}_i}} + (\boldsymbol{\lambda}_i^{\mathrm{q}})^\intercal \frac{\partial \mathbf{q}_{\mathcal{C}_i}}{\partial \mathbf{p}_{\mathcal{L}_i}} \\
&+ (\boldsymbol{\lambda}_i^{\mathrm{v}})^\intercal \frac{\partial \mathbf{v}_{\mathcal{C}_i}}{\partial \mathbf{p}_{\mathcal{L}_i}} + \rho_i(\mathbf{p}_{\mathcal{C}_i} - \mathbf{p}_{\mathcal{C}_i}^+)\frac{\partial \mathbf{p}_{\mathcal{C}_i}}{\partial \mathbf{p}_{\mathcal{L}_i}} + \rho_i(\mathbf{q}_{\mathcal{C}_i} - \mathbf{q}_{\mathcal{C}_i}^+)\frac{\partial \mathbf{q}_{\mathcal{C}_i}}{\partial \mathbf{p}_{\mathcal{L}_i}} \\
&+ \mu_i^{\mathrm{pl}} + (\mathbf{M}_{\mathcal{L}_i}^{\mathrm{vp}})^\intercal(-\underline{\boldsymbol{\mu}}_i^{\mathrm{v}} + \overline{\boldsymbol{\mu}}_i^{\mathrm{v}}) = 0
\end{aligned} \tag{21}$$

$$b_{0,i} + \mu_i^{\mathrm{pl}} = 0 \tag{22}$$

$$\begin{aligned}
&\mathbf{d}_{\mathcal{L}_i}^* + \mu_i^{\mathrm{pl}}(\mathbf{m}_{\mathcal{L}_i}^{\mathrm{pl,q}})^\intercal + \mu_i^{\mathrm{ql}}(\mathbf{m}_{\mathcal{L}_i}^{\mathrm{ql,q}})^\intercal + (\boldsymbol{\lambda}_i^{\mathrm{p}})^\intercal \frac{\partial \mathbf{p}_{\mathcal{C}_i}}{\partial \mathbf{q}_{\mathcal{L}_i}} + (\boldsymbol{\lambda}_i^{\mathrm{q}})^\intercal \frac{\partial \mathbf{q}_{\mathcal{C}_i}}{\partial \mathbf{q}_{\mathcal{L}_i}} \\
&+ (\boldsymbol{\lambda}_i^{\mathrm{v}})^\intercal \frac{\partial \mathbf{v}_{\mathcal{C}_i}}{\partial \mathbf{q}_{\mathcal{L}_i}} + \rho_i(\mathbf{p}_{\mathcal{C}_i} - \mathbf{p}_{\mathcal{C}_i}^+)\frac{\partial \mathbf{p}_{\mathcal{C}_i}}{\partial \mathbf{q}_{\mathcal{L}_i}} + \rho_i(\mathbf{q}_{\mathcal{C}_i} - \mathbf{q}_{\mathcal{C}_i}^+)\frac{\partial \mathbf{q}_{\mathcal{C}_i}}{\partial \mathbf{q}_{\mathcal{L}_i}} \\
&+ \mu_i^{\mathrm{pl}} + (\mathbf{M}_{\mathcal{L}_i}^{\mathrm{vq}})^\intercal(-\underline{\boldsymbol{\mu}}_i^{\mathrm{v}} + \overline{\boldsymbol{\mu}}_i^{\mathrm{v}}) = 0
\end{aligned} \tag{23}$$

$$d_{0,i} + \mu_i^{\mathrm{ql}} = 0 \tag{24}$$

together with complementary slackness and positive duals. Based upon the convergence of CAST, we have $\mathbf{p}_{\mathcal{C}_i} - \mathbf{p}_{\mathcal{C}_i}^+ = \mathbf{0}$ and $\mathbf{q}_{\mathcal{C}_i} - \mathbf{q}_{\mathcal{C}_i}^+ = \mathbf{0}$. By substituting (22) and (24) into (21) and (23), resp., we obtain the DLMPs for active power $\mathbf{b}_{\mathcal{L}_i}^*$ as in the distributed DLMP scheme, i.e.

$$\begin{aligned}
\mathbf{b}_{\mathcal{L}_i}^* &= b_{0,i} - b_{0,i}(\mathbf{m}_{\mathcal{L}_i}^{\mathrm{pl,p}})^\intercal - d_{0,i}(\mathbf{m}_{\mathcal{L}_i}^{\mathrm{ql,p}})^\intercal + (\mathbf{M}_{\mathcal{L}_i}^{\mathrm{vp}})^\intercal(\underline{\boldsymbol{\mu}}_i^{\mathrm{v}} - \overline{\boldsymbol{\mu}}_i^{\mathrm{v}}) \\
&- (\boldsymbol{\lambda}_i^{\mathrm{p}})^\intercal \frac{\partial \mathbf{p}_{\mathcal{C}_i}}{\partial \mathbf{p}_{\mathcal{L}_i}} - (\boldsymbol{\lambda}_i^{\mathrm{q}})^\intercal \frac{\partial \mathbf{q}_{\mathcal{C}_i}}{\partial \mathbf{p}_{\mathcal{L}_i}} - (\boldsymbol{\lambda}_i^{\mathrm{v}})^\intercal \frac{\partial \mathbf{v}_{\mathcal{C}_i}}{\partial \mathbf{p}_{\mathcal{L}_i}}.
\end{aligned} \tag{25}$$

Remark IV.1 (Cross-region injection sensitivity)**.** *Note that the sensitivities* $\frac{\partial \mathbf{p}_{\mathcal{C}_i}}{\partial \mathbf{p}_{\mathcal{L}_i}}$ *and* $\frac{\partial \mathbf{q}_{\mathcal{C}_i}}{\partial \mathbf{p}_{\mathcal{L}_i}}$ *represent the effect on the coupled injection change* $\mathbf{p}_{\mathcal{C}_i}, \mathbf{q}_{\mathcal{C}_i}$*, due to the local power injection change* $\mathbf{p}_{\mathcal{L}_i}, \mathbf{q}_{\mathcal{L}_i}$*. This couples the effect of neighboring regions into local DLMP calculations. Hence, we term this as* cross-region *injection sensitivities. In region* i*, for a coupled bus* $c_i \in \mathcal{C}_i$ *connected to* n_{c_i} *neighboring regions, the cross-region injection sensitivity can be calculated as*

$$\frac{\partial p_{c_i}}{\partial \mathbf{p}_{\mathcal{L}_i}} := \frac{\partial p_{c_i}}{\partial v_{c_i}} \frac{\partial v_{c_i}}{\partial \mathbf{p}_{\mathcal{L}_i}} = \Big(\sum_{k \neq i}^{n_{c_i}} \frac{\partial p_{c_k}}{\partial v_{c_k}}\Big) \frac{\partial v_{c_i}}{\partial \mathbf{p}_{\mathcal{L}_i}}. \tag{26}$$

Some observations regarding the above definition of $\frac{\partial p_{c_i}}{\partial \mathbf{p}_{\mathcal{L}_i}}$ *follow. In (26): (i) only voltage magnitudes are considered, as the angle differences across distribution lines are considerably smaller [2]; (ii) we incorporate information from both local* $\frac{\partial v_{c_i}}{\partial \mathbf{p}_{\mathcal{L}_i}}$ *and neighboring regions* $\frac{\partial p_{c_k}}{\partial v_{c_k}}$*; and (iii) the local sensitivities* $\frac{\partial v_{c_i}}{\partial \mathbf{p}_{\mathcal{L}_i}}$ *are obtained from* $\mathbf{M}_{\mathcal{L}_i}^{vp}$*, whereas the neighboring information* $\frac{\partial p_{c_k}}{\partial v_{c_k}}$ *is obtained in a similar way to the explicit power flow linearization.*

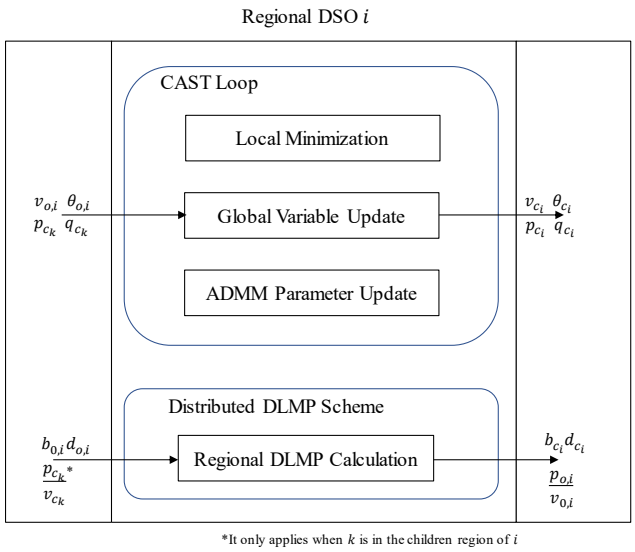

Fig. 5. Flowchart of the information exchange between regional DSOs.

B. Practical Implications

1) Inter-regional Information Flow: Building on the promise of smart grids, the proposed market framework requires a two-way communication network for all market participants. However, the type of information to be exchanged within a framework varies. For any regional DSO, Fig. 5 provides an overview of the information to be shared by a regional DSO. The communication traffic in the distributed DLMP scheme is comparably smaller than in the CAST loop since it merely requires one-time communication of passing the cleared price and cross-region injection sensitivity between regional DSOs. Note that all information except on its physically coupled buses is kept local by a regional DSO. This means that a regional DSO only needs to share information with its physically connected neighboring regional DSOs. The information needed to be revealed by any regional DSO includes physical parameters of active/reactive injections and a root-node price for its children regional DSO (only if it serves as a parent regional DSO, see Sec. IV-A for more information). This proposed information exchange framework of a regional DSO resembles a power system where multiple Regional Transmission Operator (RTOs) exist [16], [17]. Hence, the proposed framework of this paper has a high practical realization. Especially, considering that the proposed DLMP is based on a global power balance formulation (8b)

This article has been accepted for publication in a future issue of this journal, but has not been fully edited. Content may change prior to final publication. Citation information: DOI 10.1109/TSG.2019.2911996, IEEE Transactions on Smart Grid

and (8c), used for clearing LMPs at the wholesale market [3], [16].

2) Regional Real-time Market Organization: From Fig. 5, with the knowledge of its regional grid, the regional DSO can proceed to calculate DLMPs in a distributed manner. This DLMP calculation can be organized in a local market to be cleared as:

1) DGs submit their instantaneous bids, energy requirements as well as the dispatch capabilities to their respective regional DSO;
2) The regional DSO forecasts its underlying grid demand and obtains market clearing price for the root node either from wholesale market or from other regional DSOs through CAST algorithm;
3) The regional DSO clears regional DLMPs to be passed on to local DGs.

Note that the proposed market organization enables the individual market participants to make bids merely based on the local available information. Current RTO driven wholesale markets [16], [17] follow a similar information flow procedure as proposed for the above described intra-regional DSO. This shows the compatibility of the proposed method with the existing real-world electricity markets.

3) Optimality and Autonomy: Combining the above mentioned conservative inter/intra-regional information revealing properties with Remark III.1, it can also be concluded that the regional optimization steps corroborate to reach consensus, i.e., in the given feasible space, there is global convergence. On the assumption of overall social welfare maximizing DSOs and rational individual utility maximizing DGs, this convergence has also been shown to achieve the market equilibrium [7]. Hence, the proposed method achieves the overall market equilibrium of the system, while promoting the autonomy of each region.

4) Formulation Compatibility: Using linearized power flow formulations, related works exist in the form of i) proposing day-ahead markets with uncertain inter-temporal flexible loads [12] and ii) fairness-based pricing to improve the participation of market entities in DLMP programs [34], [35]. Since linearized AC power flow formulation is also deployed in the proposed CAST algorithm, these methods can be incorporated into the proposed CAST algorithm. Note that, in [12], [34], [35], network sensitivities are estimated based on DC power flow. Consequently, the resultant constraints for calculating DLMPs in [12], [34], [35] are exactly similar to (10). However, as compared to DC power flow, the AC power flow adopted in this paper is much more accurate in representing grid conditions [20] and consequently in calculating DLMPs [7]. Moreover, of relevance for the DLMP calculation, network sensitivities using linearized AC power flows for unbalanced grids have also been provided in [36]. These sensitivities for unbalanced grids can also be investigated further to be included in the proposed framework.

V. Simulation Results

We test the proposed CAST algorithm on an IEEE 33-bus system [37] with three regions as illustrated in Fig. 6 (see Scenario 1 & 2) and on a 144-bus network (see Scenario 3). Each region includes a DG operating locally. The test network has a total fixed load of 3.66 MW and 2.28 Mvar. In order to demonstrate the efficiency of the proposed method, we provide comparison against IPM of MATPOWER [38] for two realistic scenarios. For scenarios 1 and 2: the energy price at the PSP is kept at $30\,\$/\mathrm{MWh}$ and $3\,\$/\mathrm{Mvarh}$ whereas for all DGs as $20\,\$/\mathrm{MWh}$ and $3\,\$/\mathrm{Mvarh}$; voltage constraints are kept as $[0.95, 1.05]$; and the ADMM and trust-region parameters are set as: $\eta = 0.1$, $\beta = 0.9$, $\gamma = 0.5$, $\tau = 0.1$, $\kappa = 10$, $\rho_i(0) = 7 \times 10^2, \lambda_i(0) = 7, i \in \mathcal{R}$. For scenario 3, the TR parameters are kept the same while the ADMM parameters are set as: $\tau = 0.1$, $\kappa = 10$, $\rho_i(0) = 1.2{\times}10^5, \lambda_i(0) = 0.5, i \in \mathcal{R}$. The simulations are performed on a personal computer with Intel i5 2.4Ghz and 8 GB RAM.

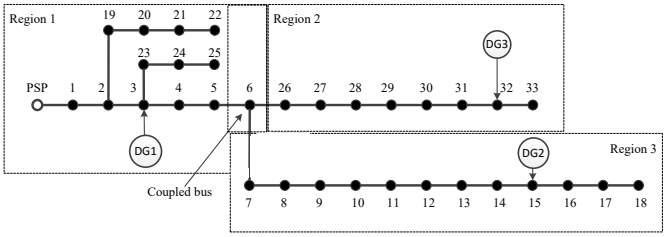

Fig. 6. 33-bus system with three regions.

A. Scenario 1 (IEEE 33-bus network)

Scenario 1 considers three DGs with identical 500 kW and ± 100 kvar capacity, i.e., with modest renewable energy penetration. The convergence of the CAST algorithm with the optimal solution is illustrated in Fig. 7 with respect to total cost, primal gap and active/reactive power dispatch. The primal gap is defined as the sum of primal residuals in eq. (14) which is a measure of disagreement on the power flow parameters of the coupled buses. In order to demonstrate the VP method in the improvement of the convergence performance, we compared the situation including/excluding the varying penalty update in closing the primal gap for all three scenarios. Note that the proposed CAST algorithm achieves the exact optimal solution as the central ACOPF (MATPOWER).

The DLMP results can be found in Fig. 8 and Table I. Since the energy supply from DGs is cheaper than the PSP, all DGs are fully dispatched (see Table II). Meanwhile, no overvoltages are caused by DGs because of the modest penetration level, keeping voltage support part of DLMP $\mathbf{\Pi}^{\mathrm{p,v}}$ at 0. Hence, the only contribution to the overall price calculation comes from the loss component of DLMPs, penalizing nodes based on their contribution to the overall losses in the distribution grid. Regarding the coupled loss component $\mathbf{\Pi}^{\mathrm{p,ADMM}}$, its value is comparatively small in contrast to local region losses $\mathbf{\Pi}^{\mathrm{p,l}}$. This shows that the effect of neighboring regions in contributing to local losses is not as great. Similar to the dispatch values, the multi-regional DLMPs are also found to be similar to the central ACOPF solution (MATPOWER).

B. Scenario 2 (IEEE 33-bus network)

In scenario 2, a high renewables-penetration level is considered by assuming 3×3 MW DG with the nominal power

This article has been accepted for publication in a future issue of this journal, but has not been fully edited. Content may change prior to final publication. Citation information: DOI 10.1109/TSG.2019.2911996, IEEE Transactions on Smart Grid

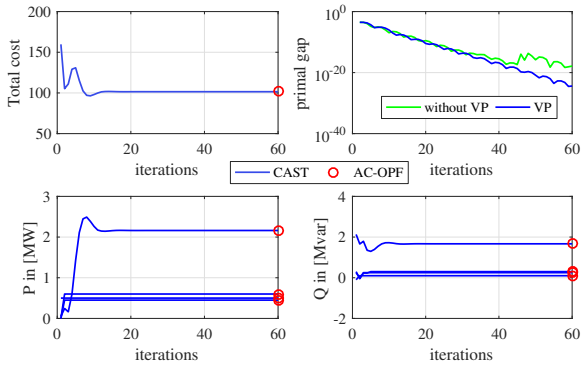

Fig. 7. Scenario 1: Convergence of CAST.

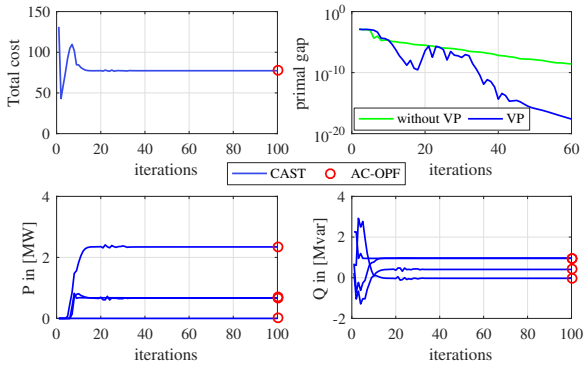

Fig. 9. Scenario 2: Convergence of CAST.

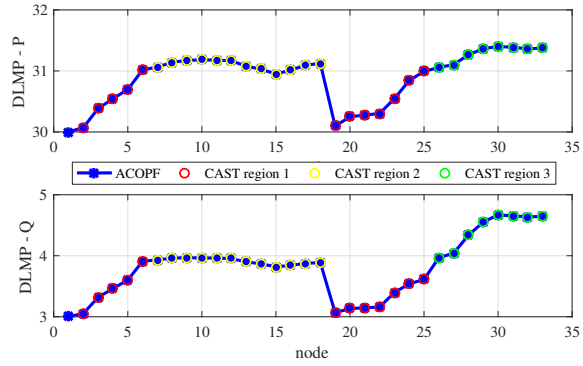

Fig. 8. Scenario 1: DLMP with ACOPF as benchmark.

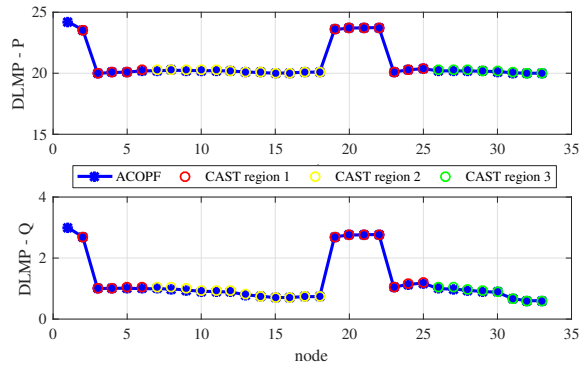

Fig. 10. Scenario 2: DLMP with ACOPF as benchmark.

Table I
ACTIVE POWER DLMPS FOR BOTH SCENARIOS

i		$\Pi^{p,e}$	$\Pi^{p,l}$	$\Pi^{p,v}$	$\Pi^{p,ADMM}$	Π^{p} (CAST)	Π^{p}(ACOPF)
3		30	0.35	0	2.8e-3	30.39	30.39
15	case 1	31.02	-0.07	0	-	30.95	30.95
32		31.02	0.35	0	-	31.36	31.36
3		24.21	-0.064	-4.15	1.2e-3	20.00	20.00
15	case 2	20.27	-0.11	-0.159	-	20.00	20.00
32		20.27	-0.062	-0.238	-	20.00	20.00

Table II
POWER DISPATCH COMPARISON OF CAST AND ACOPF

Node		P dispatch [MW]		Q dispatch [Mvar]		Total cost [$]	
		CAST	ACOPF	CAST	ACOPF	CAST	ACOPF
PSP		2.23	2.23	2.03	2.03		
DG1	case 1	0.5	0.5	0.1	0.1	103.44	103.44
DG2		0.6	0.6	0.3	0.3		
DG3		0.45	0.45	0.25	0.25		
PSP		0	0	0.95	0.95		
DG1	case 2	2.34	2.34	-0.02	-0.03	77.302	77.302
DG2		0.66	0.65	0.41	0.42		
DG3		0.69	0.69	0.94	0.94		

factor of 0.9. As a consequence, local voltages at DG buses become binding. First, we present the convergence of CAST in Fig. 9 and dispatch values in Table II. One can also observe that VP method has improved the convergence in both scenarios despite the same initial parameters. Binding voltage constraints in different regions generate more oscillations to obtain consensus among the coupled buses. The CAST settles down at a total cost of $ 77.302 which is identical to the optimal value obtained from ACOPF.

In terms of DLMP, as compared to scenario 1, the voltage support part Π^{v} is relatively high compared to other components of the DLMP that in turn reduces the DLMP at DG nodes. This penalizes DGs and reduces the local generations while maintaining the local voltage under the upper bound. Note that as nodes 15 and 32 are completely supplied by their local DGs, their cleared price $\mathbf{\Pi}^{p}$ is equal to the marginal cost of supplying power from their respective DGs, which has been set at 20 $/MWh. The dispatch results are given in Fig. 10, where it can be seen that the proposed distributed method achieves a similar quality to the central solution.

C. Scenario 3 (144-bus Network)

Table III
SCENARIO 3: DG COST AND CONSTRAINTS

Price vector	DG0(PSP)	DG1	DG2	DG3	DG4	DG5	DG6
P [$/MWh]	20	10	10	10	7	10	10
Q [$/Mvarh]	3	2	3	2	2.9	1.9	3.1
P Max [MWh]	-	1.5	1.5	1.9	1.2	2.3	1.5
Q Max [Mvarh]	-	+/-0.3	+/-0.3	+/-0.4	+/-0.6	+/-0.7	+/-0.9

In Scenario 3, we extend the test case to a larger network with 144 buses [39] . The scenario considers 5 regions with 7 DGs in total such that $\mathcal{R} = \{1, 2, ..., 5\}$. The network partition is illustrated in Fig. 11. The price vectors for the power

This article has been accepted for publication in a future issue of this journal, but has not been fully edited. Content may change prior to final publication. Citation information: DOI 10.1109/TSG.2019.2911996, IEEE Transactions on Smart Grid

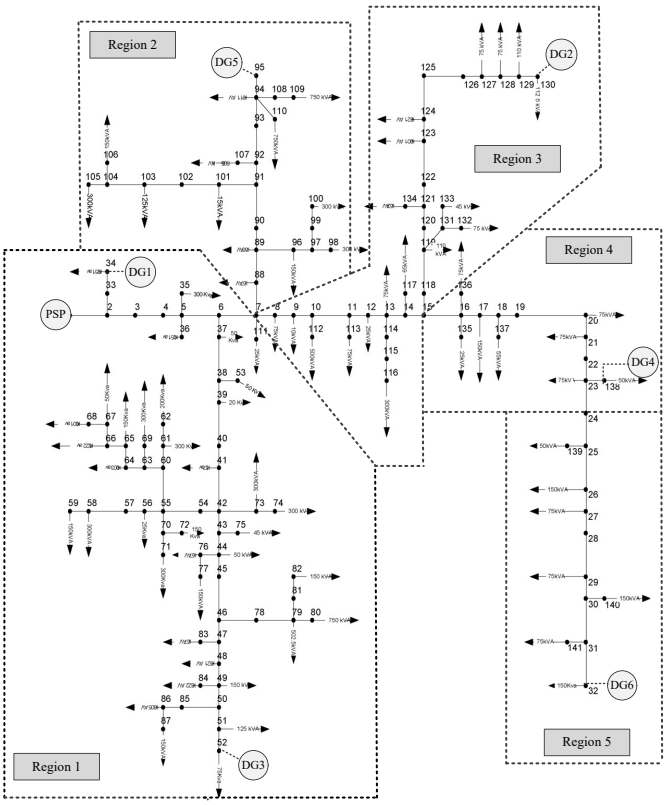

Fig. 11. 144-bus test case with 5 regions [39].

procurement from PSP and DGs are presented in Table III. The base load of the test scenario is 11.9 MW and 7.36 Mvar. The convergence of the CAST algorithm to the optimal solution is illustrated in Fig. 13 with respect to total cost, primal gap and active/reactive power dispatch. It can be seen that CAST has converged towards the same optimal solution as in ACOPF. Moreover, due to the earlier settlement for the optimal solution, one can also conclude the convergence performance is improved by VP method as well.

The test scenario considers a modest DG penetration degree, i.e., the PSP remains the primary source for the energy supply. The DLMP results for the 144-bus network can be found in Fig. 12. Since the PSP serves as the primary source for the energy supply, the DLMP is dominated by the root-node price accordingly. In general, one can observe the marginal price downstream of Region 1 is the highest due to the higher losses. On the other hand, the distributed DLMP scheme has achieved the same price accuracy as the centralized ACOPF solution, despite multiple regions and highly coupled loss terms between the regions.

D. Computation Comparison

In terms of the computation efficiency and results interpretability of the proposed method, we present the computational comparison of the local optimizer using TR, IPM and semi-definite-programing (SDP) relaxation methods in Table IV. The TR optimizer is implemented with YALMIP [40] and Gurobi [41]. The IPM and SDP are implemented with the MATPOWER interior point solver and SeDuMi [42], respectively. Note that all three solvers produce the same global solution. IPM requires less computational time than needed in TR, whereas the computational burden for SDP is the heaviest. We also notice that the computation time of TR is implementation-dependent, i.e., YALMIP consumes substantially more time in creating the model than the solver time with Gurobi. Furthermore, the DLMPs can be calculated during each iteration for the TR method, whereas it can only be recovered after finding the optimal solution for the SDP-based ACOPF and IPM-ACOPF. In this respect, a tractable formulation (i.e. a feasible power flow solution and the decomposable price signals at each iteration) can also only be provided by TR.

Table IV
COMPUTATION COMPARISON

	TR	IPM	SDP relaxation
Global solution	✓	✓	✓
Computation time (144-bus network)	2.9 s	1.3 s	12.3 s
Implicit calculation of DLMP	✓	×	×
Tractable formulation	✓	×	×

Since in the field deployment of CAST, each regional DSO solves the local problem in parallel, without extending the discussion of the inclusion of communication network, the overall solving time can be estimated by multiplying the iteration number by the local solver time. Recent works have reported a reasonable speedup of ADMM-based algorithm in a local simulation when a parallel computing technique is adopted [43].

VI. CONCLUSION AND OUTLOOK

Making full use of decentralized production, as well as flexible demand, requires a redesign of the power system. DLMPs are a major step in this direction. Nevertheless, it will be also of prime importance to combine different regions and to find a) efficient organization structures and b) efficient algorithms in order to calculate the exchange power between regions based on correct price signals. In this work, a novel decentralized market framework at a distribution grid level is proposed. The main ingredients of the framework are: (i) Consensus-Alternating direction method of multipliers Structured Trust-region (CAST) solution algorithm to capture the nonconvex AC power flow in a fully distributed way and (ii) a multi-regional DLMP decomposable pricing scheme. To demonstrate the efficiency of the proposed method, three simulation scenarios are investigated on benchmark systems, and comparisons are made to the MATPOWER state-of-the-art solver. Having proposed an efficient algorithm for decomposed pricing schemes, the reorganization of the existing power system in order to achieve both planning and operational efficiency still remains an open question and needs to be addressed in future works. Other extensions of this work may include extending the proposed method to include multi-period and multi-phase modeling.

This article has been accepted for publication in a future issue of this journal, but has not been fully edited. Content may change prior to final publication. Citation information: DOI 10.1109/TSG.2019.2911996, IEEE Transactions on Smart Grid

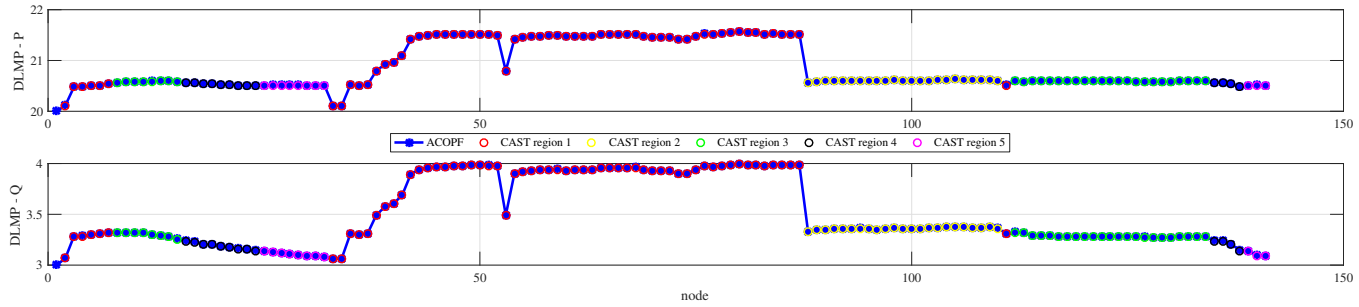

Fig. 12. Scenario 3: DLMP with ACOPF as benchmark.

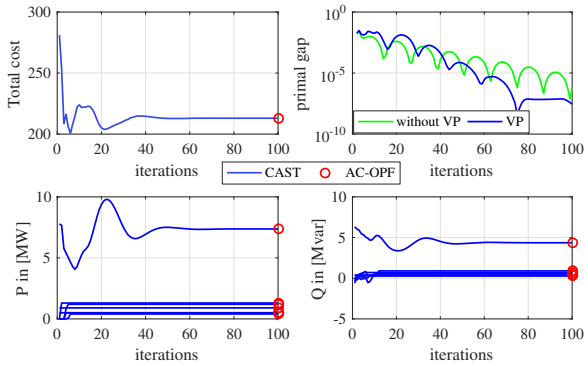

Fig. 13. Scenario 3: Convergence of CAST.

APPENDIX

A. Explicit Linearization of Power Flow in Distribution Grid

This section presents the explicit power flow linearization for the slack bus, PQ buses and the power loss. As required in the optimization problem, all linearized terms are parameterized in $\mathbf{p}_{\mathcal{L}}$ and $\mathbf{q}_{\mathcal{L}}$.

1) PQ Buses: For a given operational point $(\hat{\mathbf{v}}_{\mathcal{L}}, \hat{\boldsymbol{\theta}}_{\mathcal{L}})$, the linear estimate $(\tilde{\mathbf{v}}_{\mathcal{L}}, \tilde{\boldsymbol{\theta}}_{\mathcal{L}})$ is given as [44]

$$\begin{bmatrix} \tilde{\mathbf{v}}_{\mathcal{L}} \\ \tilde{\boldsymbol{\theta}}_{\mathcal{L}} \end{bmatrix} = \begin{bmatrix} \hat{\mathbf{v}}_{\mathcal{L}} \\ \hat{\boldsymbol{\theta}}_{\mathcal{L}} \end{bmatrix} + \begin{bmatrix} \mathbf{M}_{\mathcal{L}}^{\mathrm{vp}} & \mathbf{M}_{\mathcal{L}}^{\mathrm{vq}} \\ \mathbf{M}_{\mathcal{L}}^{\theta \mathrm{p}} & \mathbf{M}_{\mathcal{L}}^{\theta \mathrm{q}} \end{bmatrix} \begin{bmatrix} \Delta \mathbf{p}_{\mathcal{L}} \\ \Delta \mathbf{q}_{\mathcal{L}} \end{bmatrix} + \begin{bmatrix} \mathbf{m}_{\mathcal{L}}^{\mathrm{vv}} \\ \mathbf{m}_{\mathcal{L}}^{\theta \mathrm{v}} \end{bmatrix} \Delta v_0, \tag{27}$$

where $\Delta \mathbf{p}_{\mathcal{L}} := \tilde{\mathbf{p}}_{\mathcal{L}} - \hat{\mathbf{p}}_{\mathcal{L}}$, $\Delta \mathbf{q}_{\mathcal{L}} := \tilde{\mathbf{q}}_{\mathcal{L}} - \hat{\mathbf{q}}_{\mathcal{L}}$ are the active/reactive power injection variations, respectively. Sensitivity matrices $\mathbf{M}_{\mathcal{L}}^{\mathrm{vp}}, \mathbf{M}_{\mathcal{L}}^{\mathrm{vq}}, \mathbf{M}_{\mathcal{L}}^{\theta \mathrm{p}}, \mathbf{M}_{\mathcal{L}}^{\theta \mathrm{q}}$ translate the impact of PQ injections $\mathbf{p}_{\mathcal{L}}$ and $\mathbf{q}_{\mathcal{L}}$ to the voltage and angle variations and are given analytically in [44, Proposition 1]. The sensitivity vectors $\mathbf{m}_{\mathcal{L}}^{\mathrm{vv}}, \mathbf{m}_{\mathcal{L}}^{\theta \mathrm{v}}$ translate the impact of the slack bus voltage to the voltage and angles at PQ buses. Interested readers may refer [45] for the derivations.

2) Slack Bus: For the slack (root) bus, voltage v_0 and angle θ_0 are fixed. Therefore, the power flow linearization is given with respect to the nodal injections and voltage at the slack bus as

$$\begin{bmatrix} \tilde{p}_0 \\ \tilde{q}_0 \end{bmatrix} = \begin{bmatrix} \hat{p}_0 \\ \hat{q}_0 \end{bmatrix} + \begin{bmatrix} \mathbf{m}_{\mathcal{L}}^{\mathrm{pp}} & \mathbf{m}_{\mathcal{L}}^{\mathrm{pq}} \\ \mathbf{m}_{\mathcal{L}}^{\mathrm{qp}} & \mathbf{m}_{\mathcal{L}}^{\mathrm{qq}} \end{bmatrix} \begin{bmatrix} \Delta \mathbf{p}_{\mathcal{L}} \\ \Delta \mathbf{q}_{\mathcal{L}} \end{bmatrix} + \begin{bmatrix} m^{\mathrm{pv}} \\ m^{\mathrm{qv}} \end{bmatrix} \Delta v_0, \tag{28}$$

where $\mathbf{m}_{\mathcal{L}}^{\mathrm{pp}} \in \mathbb{R}^{1 \times n}$ given as

$$\begin{aligned} \mathbf{m}_{\mathcal{L}}^{\mathrm{pp}} = & (-\Re(v_0 \underline{Y}_{0,1}) \cos(\theta_1) + \Im(v_0 \underline{Y}_{0,1}) \sin(\theta_1)) \mathbf{M}_{\mathcal{L}}^{\mathrm{vp}} \mathbf{e}_1 \\ & + (\Re(v_0 \underline{Y}_{0,1}) \sin(\theta_1) - \Im(v_0 \underline{Y}_{0,1}) \cos(\theta_1)) v_1 \mathbf{M}_{\mathcal{L}}^{\theta \mathrm{p}} \mathbf{e}_1 \end{aligned} \tag{29}$$

and $\mathbf{e}_i \in \mathbb{R}^n$ is i-th entry equal to 1 and rest of the entries equal to 0. The derivation is provided as follows. In Fig. 14,

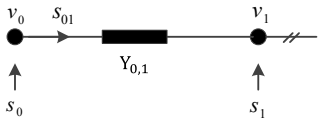

Fig. 14. Power flow linearization at slack bus.

the nodal injection at the slack bus is equal to the branch flow (i.e. $s_0 = s_{01}$), giving the following sensitivity

$$\frac{\partial p_0}{\partial \mathbf{p}_{\mathcal{L}}} = \frac{\partial \Re(s_{01})}{\partial \mathbf{p}_{\mathcal{L}}} = \frac{\partial \Re(u_0 (\underline{u}_0 - \underline{u}_1) \underline{Y}_{0,1})}{\partial \mathbf{p}_{\mathcal{L}}}. \tag{30}$$

Now, by substituting $u_i = v_i e^{j\theta_i}$ into (30) and extracting the real part, we get $\mathbf{m}_{\mathcal{L}}^{\mathrm{pp}}$. Vectors $\mathbf{m}_{\mathcal{L}}^{\mathrm{pq}}$, $\mathbf{m}_{\mathcal{L}}^{\mathrm{qp}}$, $\mathbf{m}_{\mathcal{L}}^{\mathrm{qq}} \in \mathbb{R}^{1 \times n}$ can be obtained in a similar way.

The sensitivity of slack bus injections with respect to slack bus voltage $m^{\mathrm{pv}}, m^{\mathrm{qv}}$ are derived as follows. From the power balance equation, we have

$$\frac{\partial s_0}{\partial v_0} + \frac{\partial \mathbf{s}_{\mathcal{L}}}{\partial v_0} = \frac{\partial s^{\mathrm{loss}}}{\partial v_0}. \tag{31}$$

With the PQ nodal injections remain unchanged, i.e., $\frac{\partial \mathbf{s}_{\mathcal{L}}}{\partial v_0} = \mathbf{0}$ we have

$$\frac{\partial s_0}{\partial v_0} = \frac{\partial s^{\mathrm{loss}}}{\partial v_0}. \tag{32}$$

Recalling the loss representation in (2) we obtain

$$\begin{aligned} \frac{\partial s_0}{\partial v_0} &= \frac{\partial (\mathbf{u}^{\intercal} \underline{\mathbf{Y}}\, \underline{\mathbf{u}})}{\partial v_0} = \frac{\partial \mathbf{u}^{\intercal}}{\partial v_0} \underline{\mathbf{Y}}\, \underline{\mathbf{u}} + \mathbf{u}^{\intercal} \underline{\mathbf{Y}} \frac{\partial \underline{\mathbf{u}}}{\partial v_0} \\ &= (\frac{\partial \mathbf{v}}{\partial v_0} e^{j\boldsymbol{\theta}} + j \mathbf{u} \boldsymbol{\theta} \frac{\partial \boldsymbol{\theta}}{\partial v_0})^{\intercal} \underline{\mathbf{Y}}\, \underline{\mathbf{u}} \qquad (33) \\ &\quad + \mathbf{u}^{\intercal} \underline{\mathbf{Y}} (\frac{\partial \mathbf{v}}{\partial v_0} e^{-j\boldsymbol{\theta}} - j \mathbf{u} \boldsymbol{\theta} \frac{\partial \boldsymbol{\theta}}{\partial v_0}). \qquad (34) \end{aligned}$$

Note that $\frac{\partial \mathbf{v}}{\partial v_0}, \frac{\partial \boldsymbol{\theta}}{\partial v_0}$ is the voltage and angle sensitivity with respect to v_0, i.e., $\mathbf{m}_{\mathcal{L}}^{\mathrm{vv}}, \mathbf{m}_{\mathcal{L}}^{\theta \mathrm{v}}$. Hence the slack-bus injection

with respect to slack-bus voltage is given as

$$[m^{\text{pv}}, m^{\text{qv}}] = [\Re(\frac{\partial s_0}{\partial v_0}); \Im(\frac{\partial s_0}{\partial v_0})]. \tag{35}$$

3) Losses: For loss linearization $\tilde{p}^{\text{loss}}$ and $\tilde{q}^{\text{loss}}$, we use

$$\begin{bmatrix} \tilde{p}^{\text{loss}} \\ \tilde{q}^{\text{loss}} \end{bmatrix} = \begin{bmatrix} \hat{p}^{\text{loss}} \\ \hat{q}^{\text{loss}} \end{bmatrix} + \begin{bmatrix} \mathbf{m}_{\mathcal{L}}^{\text{pl,p}} & \mathbf{m}_{\mathcal{L}}^{\text{pl,q}} \\ \mathbf{m}_{\mathcal{L}}^{\text{ql,p}} & \mathbf{m}_{\mathcal{L}}^{\text{ql,q}} \end{bmatrix} \begin{bmatrix} \Delta \mathbf{p}_{\mathcal{L}} \\ \Delta \mathbf{q}_{\mathcal{L}} \end{bmatrix}, \tag{36}$$

where the analytical representations $\mathbf{m}_{\mathcal{L}}^{\text{pl,p}}, \mathbf{m}_{\mathcal{L}}^{\text{pl,q}}, \mathbf{m}_{\mathcal{L}}^{\text{ql,p}}, \mathbf{m}_{\mathcal{L}}^{\text{ql,q}}$ are given in [7].

REFERENCES

[1] D. K. Molzahn, F. Dörfler, H. Sandberg, S. H. Low, S. Chakrabarti, R. Baldick, and J. Lavaei, "A survey of distributed optimization and control algorithms for electric power systems," *IEEE Transactions on Smart Grid*, vol. 8, no. 6, pp. 2941–2962, Nov 2017.

[2] A. Papavasiliou, "Analysis of distribution locational marginal prices," *IEEE Transactions on Smart Grid*, vol. 9, no. 5, pp. 4872–4882, Sep. 2018.

[3] M. Caramanis, E. Ntakou, W. W. Hogan, A. Chakrabortty, and J. Schoene, "Co-optimization of power and reserves in dynamic t&d power markets with nondispatchable renewable generation and distributed energy resources," *Proceedings of the IEEE*, vol. 104, no. 4, pp. 807–836, April 2016.

[4] F. Pilo and e. a. Jupe, *Working Group C6.19: Planning and optimization methods for active distribution systems*. Cigre C6, 08 2014.

[5] T. Soares, R. J. Bessa, P. Pinson, and H. Morais, "Active distribution grid management based on robust ac optimal power flow," *IEEE Transactions on Smart Grid*, vol. 9, no. 6, pp. 6229–6241, Nov 2018.

[6] S. Huang, Q. Wu, H. Zhao, and C. Li, "Distributed optimization based dynamic tariff for congestion management in distribution networks," *IEEE Transactions on Smart Grid*, pp. 1–1, 2018.

[7] S. Hanif, K. Zhang, C. Hackl, M. Barati, H. B. Gooi, and T. Hamacher, "Decomposition and equilibrium achieving distribution locational marginal prices using trust-region method," *IEEE Transactions on Smart Grid*, to be published.

[8] H. Yuan, F. Li, Y. Wei, and J. Zhu, "Novel linearized power flow and linearized opf models for active distribution networks with application in distribution lmp," *IEEE Transactions on Smart Grid*, vol. 9, no. 1, pp. 438–448, Jan 2018.

[9] L. Bai, J. Wang, C. Wang, C. Chen, and F. Li, "Distribution locational marginal pricing (dlmp) for congestion management and voltage support," *IEEE Transactions on Power Systems*, vol. 33, no. 4, pp. 4061–4073, July 2018.

[10] S. Huang, Q. Wu, S. S. Oren, R. Li, and Z. Liu, "Distribution locational marginal pricing through quadratic programming for congestion management in distribution networks," *IEEE Transactions on Power Systems*, vol. 30, no. 4, pp. 2170–2178, July 2015.

[11] Z. Yuan, M. R. Hesamzadeh, and D. Biggar, "Distribution locational marginal pricing by convexified acopf and hierarchical dispatch," *IEEE Transactions on Smart Grid*, pp. 1–1, 2016.

[12] S. Hanif, H. B. Gooi, T. Massier, T. Hamacher, and T. Reindl, "Distributed congestion management of distribution grids under robust flexible buildings operations," *IEEE Transactions on Power Systems*, vol. 32, no. 6, pp. 4600–4613, Nov 2017.

[13] S. Hanif, T. Massier, H. B. Gooi, T. Hamacher, and T. Reindl, "Cost optimal integration of flexible buildings in congested distribution grids," *IEEE Transactions on Power Systems*, vol. 32, no. 3, pp. 2254–2266, May 2017.

[14] X. Zhou, E. DallAnese, L. Chen, and A. Simonetto, "An incentive-based online optimization framework for distribution grids," *IEEE Transactions on Automatic Control*, vol. 63, no. 7, pp. 2019–2031, July 2018.

[15] Y. Lin, G. A. Jordan, M. O. Sanford, J. Zhu, and W. H. Babcock, "Economic analysis of establishing regional transmission organization and standard market design in the southeast," *IEEE Transactions on Power Systems*, vol. 21, no. 4, pp. 1520–1527, Nov 2006.

[16] W. W. Hogan, "Regional transmission organizations: Designing market institutions for electric network systems," 2000. [Online]. Available: https://tinyurl.com/yaq2ezrq

[17] USA Federal Energy Regulatory Commission: Order No. 2000, "Regional transmission organization," 1999. [Online]. Available: https://tinyurl.com/yaq2ezrq

[18] T. Erseghe, "Distributed optimal power flow using admm," *IEEE Transactions on Power Systems*, vol. 2015, no. 5, pp. 2370–2380, Sept 2014.

[19] ——, "Network reconfiguration in distribution systems for loss reduction and load balancing," *EURASIP Journal on Advances in Signal Processing*, vol. 2015, no. 1, p. 45, May 2015.

[20] S. Bolognani and S. Zampieri, "On the existence and linear approximation of the power flow solution in power distribution networks," *IEEE Transactions on Power Systems*, vol. 31, no. 1, pp. 163–172, Jan 2016.

[21] K. Turitsyn, P. Sulc, S. Backhaus, and M. Chertkov, "Options for control of reactive power by distributed photovoltaic generators," *Proceedings of the IEEE*, vol. 99, no. 6, pp. 1063–1073, June 2011.

[22] N. Hatziargyriou, *Microgrid: Architecture and Control*. Wiley, 2014.

[23] M. Rezkallah, A. Hamadi, A. Chandra, and B. Singh, "Design and implementation of active power control with improved p&o method for wind-pv-battery-based standalone generation system," *IEEE Transactions on Industrial Electronics*, vol. 65, no. 7, pp. 5590–5600, July 2018.

[24] V. Kekatos, G. Wang, A. J. Conejo, and G. B. Giannakis, "Stochastic reactive power management in microgrids with renewables," *IEEE Transactions on Power Systems*, vol. 30, no. 6, pp. 3386–3395, Nov 2015.

[25] A. Gomez-Exposito, A. J. Conejo, and C. Caizares, *Electric Energy Systems: Analysis and Operation*, 01 2008.

[26] S. Boyd, N. Parikh, E. Chu, B. Peleato, and J. Eckstein, "Distributed optimization and statistical learning via the alternating direction method of multipliers," *Foundations and Trends in Machine Learning*, vol. 3, no. 1, pp. 1–122, 2011.

[27] A. Engelmann, T. Mhlpfordt, Y. Jiang, B. Houska, and T. Faulwasser, "Distributed ac optimal power flow using aladin," in *20th IFAC World Congress*, vol. 50, no. 1, 2017, pp. 5536 – 5541.

[28] C. Song, S. Yoon, and V. Pavlovic, "Fast admm algorithm for distributed optimization with adaptive penalty," in *Proceedings of the Thirtieth AAAI Conference on Artificial Intelligence*, ser. AAAI'16. AAAI Press, 2016, pp. 753–759.

[29] W. F. Tinney and C. E. Hart, "Power flow solution by newton's method," *IEEE Transactions on Power Apparatus and Systems*, vol. PAS-86, no. 11, pp. 1449–1460, Nov 1967.

[30] J. Zhang, S. Nabavi, A. Chakrabortty, and Y. Xin, "Admm optimization strategies for wide-area oscillation monitoring in power systems under asynchronous communication delays," *IEEE Transactions on Smart Grid*, vol. 7, no. 4, pp. 2123–2133, July 2016.

[31] J. Xu, H. Sun, and C. J. Dent, "Admm-based distributed opf problem meets stochastic communication delay," *IEEE Transactions on Smart Grid*, to be published.

[32] H. J. Liu, W. Shi, and H. Zhu, "Distributed voltage control in distribution networks: Online and robust implementations," *IEEE Transactions on Smart Grid*, vol. 9, no. 6, pp. 6106–6117, Nov 2018.

[33] L. Gan and S. H. Low, "An online gradient algorithm for optimal power flow on radial networks," *IEEE Journal on Selected Areas in Communications*, vol. 34, no. 3, pp. 625–638, March 2016.

[34] S. Hanif, P. Creutzburg, H. B. Gooi, and T. Hamacher, "Pricing mechanism for flexible loads using distribution grid hedging rights," *IEEE Transactions on Power Systems*, to be published.

[35] I. Abdelmotteleb, T. Gmez, J. P. C. vila, and J. Reneses, "Designing efficient distribution network charges in the context of active customers," *Applied Energy*, vol. 210, pp. 815 – 826, 2018.

[36] S. Hanif, M. Barati, A. Kargarian, H. B. Gooi, and T. Hamacher, "Multiphase distribution locational marginal prices: Approximation and decomposition (preprint)," 2018. [Online]. Available: https://tinyurl.com/y9ged6s5

[37] M. E. Baran and F. F. Wu, "Network reconfiguration in distribution systems for loss reduction and load balancing," *IEEE Trans. Power Del.*, vol. 4, no. 2, pp. 1401–1407, Apr 1989.

[38] D. Z. Ray, E. M. S. Carlos, and J. T. Robert, "Matpower: Steady-state operations, planning, and analysis tools for power systems research and education," *IEEE Transactions on Power Systems*, vol. 26, no. 1, pp. 12–19, 2011.

[39] H. Khodr, F. Olsina, P. D. O.-D. Jesus, and J. Yusta, "Maximum savings approach for location and sizing of capacitors in distribution systems," *Electric Power Systems Research*, vol. 78, no. 7, pp. 1192 – 1203, 2008.

[40] J. Löfberg, "Yalmip: A toolbox for modeling and optimization in matlab," in *In Proceedings of the CACSD Conference*, Taipei, Taiwan, 2004.

[41] L. Gurobi Optimization, "Gurobi optimizer reference manual," 2018. [Online]. Available: http://www.gurobi.com

[42] J. F. Sturm, "Using sedumi 1.02, a matlab toolbox for optimization over symmetric cones," *Optimization Methods and Software*, vol. 11, no. 1-4, pp. 625–653, 1999.

[43] Y. Liu, H. B. Gooi, and H. Xin, "Distributed energy management for the multi-microgrid system based on admm," in *2017 IEEE Power Energy Society General Meeting*, July 2017, pp. 1–5.
[44] S. Bolognani and F. Dörfler, "Fast power system analysis via implicit linearization of the power flow manifold," in *2015 53rd Annual Allerton Conference on Communication, Control, and Computing (Allerton)*, Sept 2015, pp. 402–409.
[45] K. Christakou, J. Y. LeBoudec, M. Paolone, and D. C. Tomozei, "Efficient computation of sensitivity coefficients of node voltages and line currents in unbalanced radial electrical distribution networks," *IEEE Transactions on Smart Grid*, vol. 4, no. 2, pp. 741–750, June 2013.

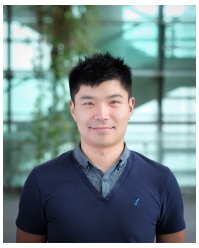

Kai Zhang (S 16) received his B.Sc. degree in electrical and electronic engineering from University of Duisburg-Essen (UDE) in 2013 and M.Sc. degree in electrical engineering and information technology from Technical University of Munich (TUM) in 2016. Since August 2016, he has been working as research associate at TUMCREATE Ltd. in Singapore and pursuing his Ph.D. His research focuses on large-scale power system optimization and energy economics.

Sarmad Hanif (M 15) is Power Systems Research Engineer at Pacific Northwest National Laboratory (PNNL). He received his B.Sc. in Electrical Engineering in 2009 from the University of Engineering and Technology Lahore, Pakistan and both M.Sc. and Ph.D. from the Technical University of Munich, Germany in 2013 and 2018, respectively. His research interests include power systems modeling and power systems economics.

Christoph M. Hackl (M'12-SM'16) was born in 1977 in Mannheim, Germany. After studying electrical engineering (controls and mechatronics) at Technical University of Munich (TUM), Germany and University of Wisconsin-Madison, USA, he received the B.Sc., Dipl.-Ing., and Dr.-Ing. (Ph.D.) degree in 2003, 2004 and 2012, respectively, from TUM. Since 2004, he has been teaching electrical drives, power electronics, and mechatronic & renewable energy systems. Since 2014, he has been the head of the research group "Control of Renewable Energy Systems (CRES)" at TUM. In 2018, he became a Professor for Electrical Machines and Drives and the head of the "Laboratory for Mechatronic and Renewable Energy Systems (LMRES)" at the Munich University of Applied Sciences (MUAS), Germany. His main research interests include nonlinear, adaptive and optimal control of electrical, mechatronic and renewable energy systems.

Thomas Hamacher is a full professor in renewable and sustainable energy systems at the Technical University Munich (TUM), Germany. His research focuses on energy and systems analysis, focusing on urban energy systems, the integration of renewable energy into the power grid, and innovative nuclear systems (including fusion). Other focuses of his work are the methods and fundamentals of energy models.